Power and Energy, Analysis, Consulting and Education, PLLC
2221 Justin Rd. #119-414
Flower Mound TX 75028
Email: ppourbeik@peace-pllc.com
www.peace-pllc.com

Developing Dynamic Load Models for the Australian Eastern Interconnected System

Prepared For:

Australian Energy Market Operator
www.aemo.com.au

Rev. #	Report Number	Date	Author(s)
1	19-05-01	4/26/19	P. Pourbeik
1.1	19-05-01	5/13/19	P. Pourbeik
1.2	19-05-01	5/20/19	P. Pourbeik
1.3	19-05-01	6/19/19	P. Pourbeik
1.4	19-05-01	6/28/19	P. Pourbeik
1.5	19-05-01	6/28/19	P. Pourbeik

Legal Notice

Table of Contents

List of Figures and Tables

1. Executive Summary

The Australian Energy Market Operator (AEMO) contacted Power and Energy, Analysis, Consulting and Education, PLLC (PEACE®) requesting that PEACE® assist AEMO in the development of a more comprehensive approach to load modeling. Presently, AEMO uses in all of its time-domain and small-signal stability analyses a simple polynomial static load model – commonly referred to in the industry as a ZIP load model. The goal of this work is to start the transition towards a composite load model that will incorporate both static and dynamic load model components. In addition, with significant penetration already, and more to come, of distributed energy sources (primarily photovoltaic residential and commercial installations) AEMO wishes to also be able to incorporate an aggregated model of the distributed energy resources (DER) into their power system simulations.

The development of a composite load model with both dynamic and static load components has been achieved, based on the data provided by AEMO. Furthermore, the so-called DER_A (distributed energy resource model A) has also been used and incorporated into the composite load model. The model when applied across the entire Australian National Electricity Market (NEM) runs well, shows no issues, and simulations for several system disturbances do not result in a significantly longer simulation time.

Moreover, simulations were performed comparing the performance of the composite load (CMLD) model to the existing AEMO static (ZIP) load model for simulating events recorded on three (3) distribution feeders, and for two (2) large system events.

The results from the distribution feeder simulations show that the CMLD model gives a much closer match of the actual load response, particularly in the reactive power (Q) response of the loads. These simulations also clearly show that the key factors in the CMLD model that have a significant influence on the performance of the model are (i) the composition numbers (i.e. what fraction of the load falls into each of the six major load components, motor A, B, C, D, power electronic and static load), and (ii) the trip settings for the various load components (i.e. the motor loads and the power electronic load).

The results from the large system disturbances also show that the CMLD model results more closely match actual system performance. However, as illustrated by some more onerous simulations (i.e. simulating bolted 3-phase faults at EHV buses) the CMLD model can result, in some cases, in seeing a fault-induced delayed voltage recovery where the EHV voltages can take up to 1 second to recover to their pre-fault levels. This delayed voltage recovery is due to the stalling of the Motor D component of the CMLD model. Moreover, based on research and development in North America, the stalling of these so-called Motor D type loads is driven by many factors, some of which cannot be truly captured in a positive-sequence simulation tool such as Siemens PTI PSS®E. For example, the rate at which the voltage drops, the point-on-wave where the fault occurs, the type of mechanical load and the configuration of transformer windings (i.e. Y-Delta etc.) can all influence what the actual motors see at their terminals down at the low voltage levels where these type motors are used, and thus drive if and how the motor stalls. As such, in the end some level of sensitivity analysis is needed when trying to capture the potential for delayed voltage recovery. Motor D type loads represent singe-phase capacitor-start induction motors that are used in residential and light-commercial loads such as air-conditioning,

1

refrigeration, heat-pumps etc. Based on the initial survey and data mining done by AEMO, the percentage of such loads (Motor D component) has been estimated at between 3 to 6% across Australia. This is because, it is believed that the majority of air-conditioning load in Australia is inverter-based (i.e. similar to power electronic loads). Thus, again this highlights the need for more investigation in the future in understanding the actual load composition today and how it might evolve in the near future in Australia.

Thus, in summary it may be said that the CMLD load model does make simulations more closely match measured system response, but in addition when modeling 3-phase faults (as is done typically in transmission planning studies, while in real-life 3-phase fault are rare) the simulation results for system voltage recovery will be more pessimistic with the CMLD model than they have been in the past with the existing AEMO static-load model.

The CMLD model has been available in Siemens PTI PSS®E (and several other simulation platforms in North America) for several years. The standalone DER_A model has also been available in these commercial tools, and tested in North America, for close to a year. However, the combination of the two models into a single comprehensive aggregated model to represent both load and DER at the end of an aggregate feeder was just very recently (early June, 2019) tested as a beta version across the North American simulation tools within the WECC Modeling and Validation Working Group. As such, this combined model that was used here for simulating the combination of CMLD and DER_A, is based on the latest beta release from Siemens PTI PSS®E in Version 34.5.1.

Thus, the combination of CMDL and DER_A was then used to simulate a few distribution-feeder events and one large system wide event.

For the distribution events, it was seen that a relatively good match could be achieved with the combination of the CMDL + DER_A model, with some adjustment to the parameters. This includes seeing the DER momentarily blocking and then coming back up, and some possibly tripping, as seen in real events. Of course, the ZIP model (nor the CMLD model by itself) cannot emulate any of this behavior.

For the system wide event, the key observations were that: (i) the existing static (ZIP) load model again depicts a quick return of the system voltage, with some sharp over-voltages, that do not resemble the actual measured system behavior, (ii) that the general slower recovery rate and more smooth response of the CMLD+DER_A model is more believable, and as the composition parameters are improved in the future, they may render even more promising results, and (iii) the combined CMLD + DER_A model behaved well in the simulation and did not significantly affect the simulation time for simulating the event as compared to the existing static load model.

All of the above said, the following general conclusions and recommendations can be made:

- To improve the parameterization of the CMLD and DER_A models, AEMO should consider doing a more thorough and up-to-date (i.e. based on 2018 data perhaps) survey of the loads in the Australian system, and/or working with entities like the CSIRO to come-up with more up-to-date composition data on the residential and commercial loads across the regions in Australia, and if possible at a little more granular level – e.g. based on general climate zones.

- To thus update the load composition percentages, and come up with percentages for a wider range of seasons/times of the year and times of the day for planning studies.
- To try to explicitly model large industrial loads such as mining where this is plausible and more specific and detailed data on such loads can be obtained.
- To perform sensitivity analysis to identify the key parameters that the Australian system is most sensitive to in the CMLD model, and to thus in the process of the surveying identify physically meaningful boundaries and ranges on these parameters. Based on the limited analysis here, and some engineering judgment, it can be said at a first cut that the most sensitive parameters are, the composition fractions (*Fma, Fmb, Fmc, Fmd, Fel*) and the trip settings on the various load components.
- To survey in more depth the installed PV throughout the system and to be able to clearly cross-reference the installed capacity with the specific power flow bus numbers in the base cases developed. Also, a process needs to be put in place to regularly monitor and update these as PV installations continue to increase. Furthermore, it would be beneficial to develop some simple automated routines to generate the PV records and populate them into the power flow records (see what needs to be done as described in section 7.4) to simplify this process. Moreover, the DER_A parameters used here where those representing PV installations post-2015 (for the sake of simplicity). As AEMO embarks on using the CMLD**DGU2 model, and performs more detailed surveys of the deployment of DG on the AEMO system, attention should also be given to identifying the exact mix of PV characteristics (i.e. those that meet the 2015 performance requirements and those that do not). Thus, the appropriate parameters will need to be used, and refined as more experience is gained.
- The present AEMO NEM Siemens PTI PSS®E model is severely lacking in proper turbine-governor modeling for the vast majority of synchronous generators on the system. This deficiency of the Australian system model will need to be first addressed before one can rely on any results that may pertain to system wide frequency events.
- Given the fact that AEMO performs many of its studies in EMT modeling tools (i.e. PSCAD), particularly for low system short-circuit strength regions, it may be prudent to develop an aggregated DER model, similar to DER_A, in the PSCAD environment, as well as the CMLD type aggregate load model structure. This would need some significant time to develop and test and benchmark.
- To take a closer look at the distribution parameters of the CMLD model for each region in the Australian NEM system.
- There may be value in introducing more high-speed monitoring (e.g. digital-fault recorders, which are PMU capable) both at load centers, as well as at key transmission nodes and generating station in order to increase the fidelity of the measured event data for future refinement of models through comparing simulations to measured event data.

Finally, it should be emphasized, as illustrated even by the initial work here, that there can never be "one" highly accurate load model, due to the constantly changing nature of the load and the countless variety of load components, as well as the variability in the PV

generation. Thus, when performing planning studies, a level of sensitivity analysis needs to be performed around both load model composition and the load component trip settings. Such sensitivity analysis, must however, incorporate engineering judgement in that (i) variations in the composition numbers should be based on survey data to ensure that unrealistic numbers are not used, and (ii) sensitivity analysis may only be needed when looking at the most onerous system conditions and contingencies.

For futuristic planning studies AEMO may need to consider working with consultants and firms with expertise in solar forecasting, in order to develop realistic PV penetration scenarios under various potential weather patterns for system planning studies.

2.   Introduction

The Australian Energy Market Operator (AEMO) contacted Power and Energy, Analysis, Consulting and Education, PLLC (PEACE®) requesting that PEACE® assist AEMO in the development of a more comprehensive approach to load modeling. Presently, AEMO uses in all of its time-domain and small-signal stability analyses a simple polynomial static load model – commonly referred to in the industry as a ZIP load model. The goal of this work is to start the transition towards a composite load model that will incorporate both static and dynamic load model components. In addition, with significant penetration already, and more to come, of distributed energy sources (primarily photovoltaic residential and commercial installations) AEMO wishes to also be able to incorporate an aggregated model of the distributed energy resources (DER) into their power system simulations.

The remainder of this report is organized as follows:

Section 3 – gives an overview of composite load modeling, in order to include both load model dynamic and static behavior.

Section 4 – provides a detailed description of the development of an initial composite load model (CMLD) for the AEMO system in Siemens PTI PSS®E.

Section 5 – provides a summary of comparisons between simulations and measured events at three load feeders, in order to assess the performance of the CMLD load model.

Section 6 – provides a summary of comparisons between simulation and measured events for a couple of large system events, using the CMLD model on the entire Australian power system model.

Section 7 – provides the results for the comparison between simulation and measured events for both distribution and large system events, using both the CMLD model and the new DER_A model for modeling distributed solar photovoltaic (PV) generation.

Section 8 – provides a summary of the entire work with some recommendations for possible future efforts by AEMO.

3.   The Composite Load Model

Modeling of the behavior of end-use loads in time-domain stability simulations, remains perhaps as the single most challenging task in developing transmission planning models for planning and operational studies. The complexity of load modeling is driven by two main factors:

   i.   the behavior of the load, as seen on the extra high voltage (EHV) transmission systems, unlike other power system components like generation, is an aggregation of countless small end-use devices on the distribution system,

   ii.   the composition of the load is constantly changing.

With respect to the latter point above, this change has several dimensions. First, the load composition is constantly changing due to hourly variations in customer usage. Secondly, there are seasonal variations in the load composition, for example, residential load may be dominated by air-conditioning load during summer months. Thirdly, the nature of the load and load characteristics change over the course of many years as the technologies associated with the end-use load change. For example, over the last decade, incandescent lighting has been almost entirely phased out in many countries around the world, including USA[1], Australia[2] and many European countries in efforts to improve energy efficiency. Finally, there is the issue of demographic variations in load characteristics. For example, a load pocket dominated by residential loads will have quite different composition and characteristics to a load pocket that is dominated by industrial or commercial loads.

Another aspect of the ever-changing load characteristics around the world, particularly in certain regions of North America, Europe and Australasia, is the huge influx of distributed energy resources (DER), particularly residential roof-top solar photovoltaic (PV) systems, electric vehicles and small battery energy storage systems. To this end the modeling of load becomes an exercise of modeling both load and DER.

Thus, there is no one load model that can be used for simulations under all conditions, but rather modeling load ultimately is an exercise of developing a reasonable representation of the load on the system for the various seasonal time frames to be studied, and to attempt to remain diligent with updating the load model as the end-use loads and technologies change over time. Furthermore, some level of sensitivity analyses will be needed over the range of parameters that are most critical to system performance.

Presently, the most advanced dynamic load model available is the so-called composite load model (*cmpld*) developed initially by the Western Electricity Coordinating Council's (WECC) Modeling and Validation Working Group (MVWG)[3]. This model is presently available in many commercial software platforms, including Siemens PTI PSS®E, GE

---

[1] *Paul Davidson (16 December 2007). "It's lights out for traditional light bulbs". USA Today. Archived from the original on 26 June 2012.*

[2] *"Phase-out of inefficient incandescent light bulbs". Think Change. Department of Climate Change and Energy Efficiency. 2 February 2011. Archived from the original on 1 May 2011. Retrieved 15 May 2011.*

[3] https://www.nerc.com/comm/PC/LoadModelingTaskForceDL/Dynamic%20Load%20Modeling%20Tech%20Ref%202016-11-14%20-%20FINAL.PDF

PSLF^{TM}, PowerWorld Simulator and PowerTech Labs TSAT^{TM}. The model structure is shown below in Figure 1. AEMO licenses and uses Siemens PTI PSS$^®$E.

A few comments are pertinent at this point about the *cmpld* model. It has been in use by WECC since 2013, at which time a phased approach was taken to slowly phase in the *cmpld* model fully into planning studies. The full model has been used since about 2016. Also, since late 2016, early 2017 the North American Electric Reliability Corporation (NERC) has been encouraging its use throughout North America [1]. Moreover, the Electric Power Research Institute (EPRI) has spent significant time and research funds in benchmarking the *cmpld* model across all the major commercial software tools in North America, and thus helped to find some inconsistencies in model implementation and therefore helped to bring the software implementations closer together and more consistent with one another. These efforts have been reported on in the various WECC and NERC load modeling task force meetings. The above said, the latest and most tested version of the composite load model in Siemens PTI PSS$^®$E is available in Version 34.5.1 of the tool[4].

Consider Figure 2, which shows the structure of the *cmpld* model. The parts of the model are as follows:

1. The representation of the distribution transformer (*jXxf*) together with the on-load tap-changer (OLTC), if there is an active OLTC.
2. The representation of any explicit substation shunt capacitors (*Bss*).
3. A single equivalent representation of the distribution feeders that feed the actual end-use loads (*Rfdr + jXfdr*). The feeder compensation (*Bf1* and *Bf2*) are not user input, but rather calculated internally by the model to balance out the reactive losses on the feeder etc. to ensure that the net load MW/MVar at the transmission bus matches that in the power flow case.
4. Finally, a number of load component models at the end of the equivalent feeder, which in an aggregated way, emulate the behavior of the various load components. There are the three (3) three-phase induction motor models (Motor A, B and C), the performance model representation of residential air-conditioning load (Motor D), and the power electronic and static load model components.

Motor D is a specially developed performance model of single-phase residential air-conditioning loads based on laboratory tests of such devices [2]. It is, however, used in general to represent other single-phase induction motor residential loads such as refrigeration compressor motors. More recently efforts in the WECC have focused on developing a DER model to include also in this composite load model [3] as shown in red in Figure 1.

---

[4] Moreover, the version used here has some additional minor improvements which were made by Siemens PTI and shared with us in an updated DLL of Version 34.5.1, which is no doubt available to all user's upon request and to be released in the next minor release of the program.
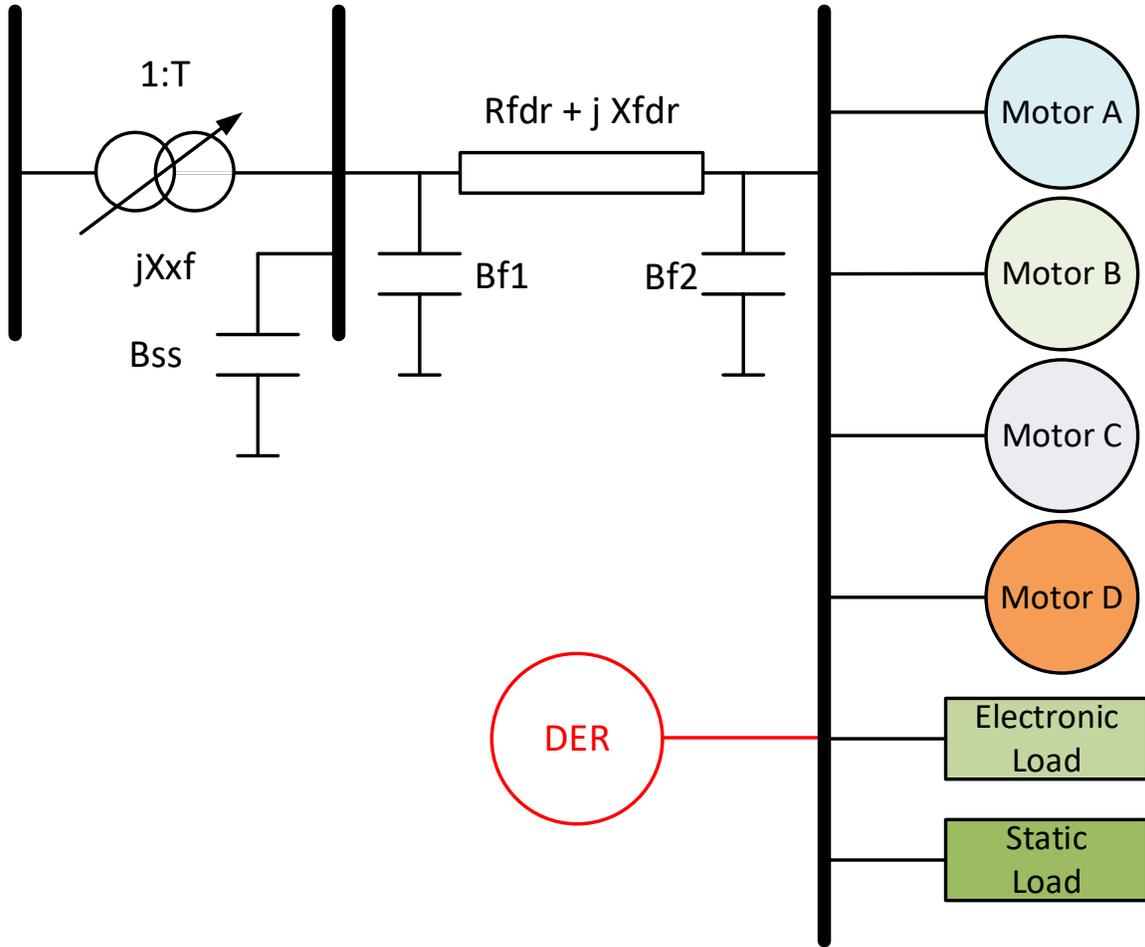
Figure 1: The composite load model (cmpld) structure.

In developing parameters for the composite load model, presently the most sophisticated approach is taken by WECC, and may be generally summarized as follows:

1. The parameters associated with the individual components (e.g. electrical parameters of the 3-phase motors A, B and C, those of the performance model of the single-phase motor D, etc.) are essentially fixed and are based on an average observed behavior of some of the components based on extensive laboratory tests (e.g. for the residential a/c compressor motors [2]) or based on extensive surveys conducted on various commercial and industrial facilities [4].

2. Through extensive work in WECC the region has been divided into various climate zones and thus, based on the climate zones, and the time of year and time of day the percentage of the Motor A, B, C and D fractions, and the fraction of power electronic loads and static load is tabulated.

3. The two pieces above then together make up the *cmpld* model data card for each bus based on its climate zone designation and the season and time of day chosen for the simulation to be performed.

All of the above is done using a tool maintained and developed by the Pacific Northwest National Labs, called LMDT[5].

The most challenging part of the above process, which in the end has associated with it some engineering judgment, is going from the load composition to the fractions of the load model components. That is, utilities are often able to go through surveys and look at actual metered end-use data to determine what percentage of the load consumption is residential, commercial and industrial load. This data then needs to be translated into the fractions of the Motor A, B, C, D, power electronic load and static load representations in the *cmpld* model. Developing such so-called rules of association require again much surveying of various load pockets, and some judgement and assumptions. One of the most comprehensive such studies, that is publicly available, is that which was funded by Lawrence Berkeley National Laboratory in 2014, for the New England area in the US [5].

The above described approach is commonly referred to as a component-based approach to load modeling.

Another approach is a so-called measurement-based approach [6]. The measurement-based approach, however, has a few limitations. First, the need for a significant amount of measurement data from various locations in the power system and for various times of the year, and for disturbances that do not have more than 10% or so unbalance among the phases. Secondly, the general difficulty with dealing with multiple solutions that come out of an optimization process and the need for having some general baseline information to guide the optimization process towards a physically meaningful result.

In the end, ideally a combination of both approaches above is likely to lead to greater fidelity in load model development.

Finally, no matter how extensive the process for load modeling development is, load models must always be accompanied in transmission studies with some level of sensitivity analysis, since as mentioned at the onset of this brief discussion the system load is never constant and so there is always some level of uncertainty in the load model parameters.

With this brief background in mind, this general approach was taken in this work to come up with a reasonable first attempt at a composite load model for the Australian Eastern Interconnection, using the data presently available and at the disposal of AEMO.

---

[5] https://svn.pnl.gov/LoadTool

4.   Developing a Composite Load Model for AEMO

Here we describe the steps taken, in close collaboration with AEMO staff, in coming up with a first version of a composite load model to be used by AEMO in the Australian Eastern Interconnection model in Siemens PTI PSS®E. As mentioned in the previous section, the most advanced composite load model structure presently available in Siemens PTI PSS®E (and several other commercial tools) is that shown in Figure 1, initially develop in WECC. In Siemens PTI PSS®E this model is called CMLDxxU2[6].

As explained briefly in the previous section, the approach here was the so-called component-based approach, together with an attempt at the end to compare simulations with some measurement data provided by AEMO. Thus, the following steps were taken:

1. Step 1: AEMO staff using data from several sources within Australia came up with the load composition on a state by state basis for each of the five (5) areas in the Australian Eastern Interconnection, i.e. Queensland (QLD), New South Wales (NSW), Victoria (VIC), South Australia (SA) and Tasmanian (TAS) – see Figure 2.
2. Step 2: AEMO staff then computed a first estimate of the percentages of Motor A, B, C, D and power electronic load fractions, as well as the ZIP load components by applying the rules of association published in [1] and [5], to the composition data compiled by AEMO in step 1. The results of these two steps was then provided to PEACE® in a spreadsheet[7].
3. Step 3: PEACE® reviewed briefly the spreadsheet provided and we made one change. With the exception of the construction and conventional boiler categories, for all the other large industrial loads (LILs) we changed the rules of association tables in AEMO's spreadsheet such that the remaining fraction of load is applied to the constant current load category as opposed to constant impedance, as originally designated by AEMO[8]. To explain this change, consider that in Table 7 of reference [1], which is what is being used by AEMO as the rules of association (ROA) for LILs, the fraction of ZIP loads is not provided. The reference simply states that the remainder of the load fraction should to apply to a static load model. Thus, AEMO applied the remainder to a constant impedance model. However, in general the majority of the remaining load in industrial facilities (i.e. what load that remains after accounting for all motor loads, power electronic loads, etc.) is lighting. Furthermore, the majority of lighting that is used in industrial and are commercial facilities is fluorescent lighting, which is closer to a constant current load type.

    Aside Important Notes: The Motor D category, as explained in section 3, was created in WECC primarily to account for the compressor motor load on residential air-conditioning (a/c) load in North America. In North America, almost without

---

[6] The version of Siemens PTI PSS®E being used here is Version 34.5.1 released on November 30th, 2018, together with some additional slight modifications released to us by Siemens PTI in updated DLLs on April 19, 2019.

[7] *2019-04-05-Load Composition Overview.xlsx*

[8] See column I and J of the LILs RoA tab in *2019-04-05-Load Composition Overview_Modified_V1.0.xlsx*

exception, all residential a/c (even on new construction to-date) use a conventional cross-the-line, capacitor-star, conventional single-phase induction motor. These are very prone to stalling, under certain conditions, and so can be a huge draw of reactive and active power on the grid when they stall. In contrast, many other countries, such as Australia, tend to use inverter-interfaced motors that are more efficient and not susceptible to stalling, but behave closer to an electronic load. This was discussed with AEMO, and thus it is our understanding that AEMO took this into consideration in adjusting some of the rules of association for the residential loads. Thus, the small remaining Motor D fractions are associated with single-phase induction motor loads associated with refrigeration and what might exist in some small fractions elsewhere. Also, many of the survey and input data used by AEMO is a few years old and so moving forward some of the input data might be updated in the future to reflect other changes in load profile, such as the move away from incandescent to LED and CFL lighting in recent years. This will need to be done in the future.

4. Step 4: Using the composite load model fractions derived at the end of step 3, we thus developed the CMLD model for each of the five regions on the Australian Eastern Interconnection. This step, and assumptions made to achieve this, are explained in more detail below.
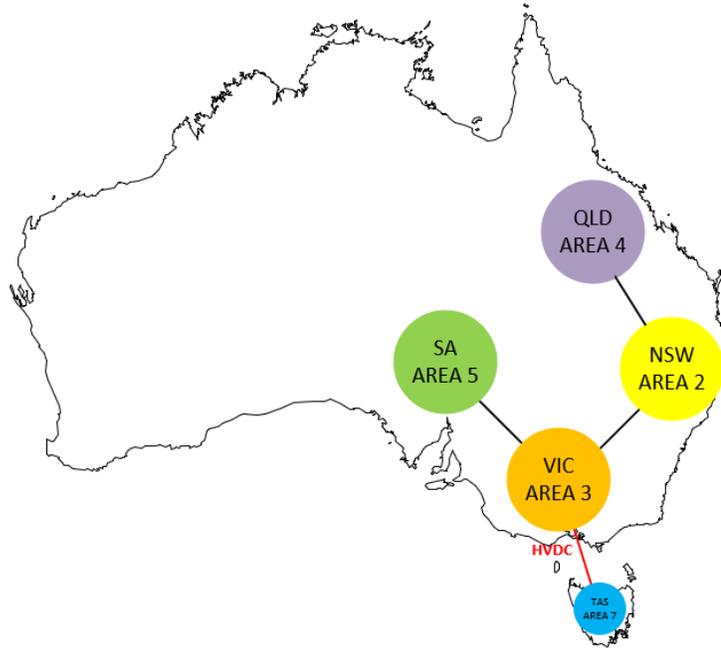
Figure 2: The five (5) areas in the Australian Eastern Interconnection.

4.1   Developing the Composite Load Model Records

As explained above, based on the extensive work done by AEMO internally, and a few minor modifications (Step 2 and 3 in the above) the composite load model component fractions were derived. These are shown Table 1 and

Table *2* for summer and winter evening peaks, respectively[9]. Using these numbers, we can now develop the CMLD model records in Siemens PTI PSS®E.

Table 1: Summer evening peak load component fractions

	Motor A	Motor B	Motor C	Motor D	Power Elec	Constant Current	Constant Impedance
QLD	12%	14%	10%	3%	27%	16%	18%
NSW	12%	10%	9%	6%	24%	14%	25%
VIC	12%	10%	6%	6%	26%	16%	24%
SA	9%	13%	11%	5%	35%	7%	20%
TAS	14%	12%	13%	3%	15%	27%	16%

Table 2: Winter evening peak load component fractions

	Motor A	Motor B	Motor C	Motor D	Power Elec	Constant Current	Constant Impedance
QLD	6%	12%	11%	3%	19%	19%	30%
NSW	4%	8%	8%	6%	20%	17%	37%
VIC	4%	8%	7%	6%	20%	20%	35%
SA	5%	12%	11%	6%	26%	8%	32%
TAS	8%	11%	11%	4%	15%	25%	26%

However, before developing the CMLD records some key items should be noted:

1. Here we will use the CMLDZNU2 model, which is the Zone wide version of the model. That is, all loads in a given Zone of the power flow model will be converted to the same model as defined in the data card.
2. The CMLD model cannot deal with loads that have a negative real (MW) component. This is understandable, since associating a negative real power to motor loads (particularly Motor D) can easily result in nonsensical results. Thus, we must remove all such loads to a separate zone and not associate CMLD with them.
3. It is equally unwise to associated CMLD with load that have a large negative reactive power (MVar) component and/or have a large Q/P ratio. That is, the load in power flow has much larger reactive power than real power. Currently, the CMLD model (based on our discussions with Siemens PTI) is hard coded such that it will not be applied to loads with a Q/P ratio greater than 4, or $P < 0.5$ MW.
4. For loads that are modeled in the power flow case to be on the distribution voltage (i.e. the distribution transformer is already explicitly modeled in the power flow case) should not model the distribution transformer in the CMLD model (i.e. set *Xxf* = 0).

Some of these items are being worked on by Siemens PTI so that in future releases of the model, global threshold variables can be set by the user to cater for these issues. However, for now we dealt with these items by creating different zones for the loads in the power flow case as explained below.

---

[9] The numbers in the tables for constant current and impedance loads have been rounded up to ensure that each row adds up to 100%. This was done in order to provide the numbers in whole integer percentages.

To test the CMLD model, we started with one of the snap shot cases provided by AEMO, namely *20180104-203047-SubTrans-5digit-SystemSnapshot.sav*.

Before applying the CMLD model to the case the following changes were made to the power flow case:

1. We noticed that in the original base case all loads are in one of two zones:
    a. Zone 1 – the majority of these are negative loads and they appear to be associated with wind and solar power plants. These are all left in Zone 1 and no CMLD model associated with them
    b. Zone 99 – all other loads.
2. All loads in Zone 99 were moved to newly created zones as follows:
    a. Zone 88 – all load with either a negative real and/or reactive part
    b. Zone 49 – all QLD loads lumped up onto the EHV buses
    c. Zone 40 – all QLD loads lumped onto distribution buses (11, 22 and 33 kV)
    d. Zone 44 – all power plant auxiliary loads in QLD
    e. Zone 29 – all NSW loads lumped up onto the EHV buses
    f. Zone 20 – all NSW loads lumped onto distribution buses (11, 22 and 33 kV)
    g. Zone 22 – all power plant auxiliary loads in NSW
    h. Zone 39 – all VIC loads lumped up onto the EHV buses
    i. Zone 30 – all VIC loads lumped onto distribution buses (11, 22 and 33 kV)
    j. Zone 33 – all power plant auxiliary loads in VIC
    k. Zone 59 – all SA loads lumped up onto the EHV buses
    l. Zone 50 – all SA loads lumped onto distribution buses (7.5, 11 and 33 kV)
    m. Zone 55 – all power plant auxiliary loads in SA
    n. Zone 79 – all TAS loads lumped up onto the EHV buses
    o. Zone 70 – all TAS loads lumped onto distribution buses (11, 22, 33 and 44 kV)
    p. Zone 77 – all power plant auxiliary loads in TAS

A few further comments are also worth noting here:

a. The loads that have been placed in Zone 88, in some cases, may not be real and could perhaps be further refined and recategorized. For now, we have not attempted this apart from two obvious ones. Two rather large negative loads were turned off and their values subtracted out of the other large positive loads on those same buses.
b. For the loads that were moved to Zones 40, 20, 30, 50 and 70 (on distribution buses) there were some on even lower voltage levels, but very few. Also, it was assumed that the distribution voltages were 44 kV and lower. All loads at 66, 110, 132, 220, 275, 330 and 500 kV were placed in zones 49, 29, 39, 59 and 79.

With these changes made to the base case the load was thus modeled as follows:

1. All loads in Zones 49, 29, 39, 59 and 79 were modeled with the CMLDZNU2[10] model and with the component fractions as shown in Table 1, since this is a summer power flow case.

---

[10] In the work performed here the CMLDZNU2 model is used, which applies the same set of CMLD model parameters to all loads in a given Zone. There are several versions of the model CMLDBLU2 (applied to a bus), CMLDOWU2 (applied to an owner number), CMLDZNU2 (applied to a zone number), CMLDARU2

2. All loads in Zones 40, 20, 30 50 and 70 were also modeled as above with one difference, the distribution transformer model in CMLD was nulled out (removed) by setting the parameter *Xxf* = 0.
3. All loads in Zones 44, 22, 33, 55, and 77 were modeled using the NERC component fractions for power plant auxiliary loads, as shown in Table 3.
4. All other loads (in Zone 1 and 88) were modeled using AEMO's existing static load model parameters.

Table 3: Power plant auxiliary load component fractions (from Table 7 of [1]).

	Motor A	Motor B	Motor C	Motor D	Power Elec	Constant Current	Constant Impedance
Power Plant Aux. Load	5%	50%	25%	0%	15%	5%	0%

The final files produced are:

Power Flow Case: *20180104-203047-SubTrans-5digit-SystemSnapshot_NewZones_042419.sav*

Dynamics Case: *20180104-203047-SubTrans-5digit-SystemSnapshot_WithCMLD_042419.dyr*

The *Cnv_NEM_Loads_v2.py* file (supplied by AEMO) is still used to convert all remaining loads (Zone 1 and 88) to the AEMO static load models and perform some other necessary tasks before initialization.

4.2 The Parameters of the CMLD Model

As explained in section 3, and shown in Figure 1, the CMLD model incorporates eight (8) major elements:

1. a model of a distribution transformer,
2. a model of an equivalent distribution feeder,
3. three (3) models of aggregated 3-phase induction motor loads (Motor A, B, C),
4. a performance model of an aggregated representation of single-phase induction motors, primarily developed to represent residential 1-phase a/c compressor motors (Motor D),
5. an aggregated model of power electronic loads (PEL), and
6. an aggregated model of all remaining static, voltage and frequency dependent, loads (ZIP).

The complete list of parameters of the *CMLD**U2* model in Siemens PTI PSS®E version 34.5.1 is provided in Appendix A, together with the parameter values used here. This should be explained.

The nine (9) parameters highlighted in **orange** and left blank in Appendix A are the key parameters that come from a component or measurement-based load composition derivation effort. These are the fractions of the load that are to be represented as Motor A (FMA), Motor B (FMB), Motor C (FMC), Motor D (FMD), PEL (FEL) and static load (P1s/Q1c and P2c/Q2c). The method by which the static-load parameters are calculated is shown in the table. Thus, these nine parameters come directly from the load component

---

(applied to an area number), CMLDALU2 (applied to all loads). The order of precedence is the bus model has the highest precedence followed by owner, zone, area and then all.

composition work described in section 4.1, and thus shown in Table 1, Table 2 and Table 3.

The first parameter, load MVA base, is typically set to -0.8 in North America. What this means is that the MVA based of the load is calculated to be = |Load MW|/0.8. This based on a broad assumption that most typical distribution transformers and feeders are rated to be at least 1.25 times greater in rating than the maximum load on the distribution transformer. If a better estimate is available it can be used. Note: if this parameter is set to a positive value, then that value is used as the fixed MVA base. Negative values are used as indicated here as a loading factor. For the Zone (or area, or owner, or all) CMLD model (i.e. CMLDZNU2) used here, this parameter has to be a loading factor (i.e. negative number).

The second parameter is for modeling explicit shunt capacitors that may be known to exist on the low-voltage bus of the distribution transformer. This is typically left as zero, especially when using the Zone wide CMLD model.

The Distribution Transformer and Feeder Model:

The next sixteen (16) parameters (J+2 to J+17) represent the distribution transformer and equivalent feeder model. These have been explained in the comments section of the table in Appendix A. These have been set to typical values, which based on our brief discussions with AEMO seem reasonable for the Australian system as well. A few of the parameters have been highlighted in **green**. These can possibly be further refined for each of the five regions in Australia based on further discussions with distribution engineers. These are:

- The equivalent feeder impedance. It has been assumed that the total aggregated equivalent feeder impedance as seen from the substation is 0.04 pu on the load MVA with an X/R ratio of 1. It should be noted that most lines/cables used for distribution do have a low X/R ration, so this assumption is probably reasonable.
- Parameter *Fb* (J+4) is simply an educated guess of where to place the majority of the distribution capacitors. When the power system model is initialized within Siemens PTI PSS®E, the CMLD model is applied to all the loads to which it has been assigned. It is essential that the net MW/MVar load, upon initialization, be equal to the MW/MVar of the lumped load value in the power flow tables. Thus, during initialization, the value of the total feeder reactive compensation (*Bf1 + Bf2*, in Figure 1) is calculated to balance the reactive consumption of the load devices and of the transformer and feeder with the total load Q value originally specified in the power flow tables. Thus, *Fb* determined the distribution of the shunt compensation (i.e. *Bf1 = Fb×(Bf1+Bf2)* and *Bf2 = (1 – Fb)×(Bf1+Bf2)*).
- The remaining parameters, which are parameters of the distribution transformer, are self-explanatory (see Appendix A). These have been set to typical values which AEMO has also confirmed as reasonable for their system. That is, a leakage reactance of 8% for the distribution transformer, and an on-load tap-changer (OLTC) range of 1.1 to 0.9 with each tap step being 0.00625 pu. It is also assumed that the OLTC tries to maintain the distribution voltage between 1 to 1.02 pu. The only caveat is that the distribution transformer can be altogether eliminated from the model by setting *Xxf* = 0. This is done for example in the AEMO case in what we have designated as Zones 20, 30, 40, 50 and 70, where the distribution

transformers at these load buses are already explicitly modeled in the power flow case.

- Finally, to disable the OLTC action both during initialization and dynamics, set parameter J+8 = 0.

The Power Electronic Load (PEL) Model:

Parameters J+23 (*PFel*), J+24 (*Vd1*), J+25 (*Vd2*) and J+132, are all associated with the PEL. For PEL the load power factor is assumed to be 1 (J+23). This is because although PEL do not necessarily truly have a power factor of 1, due to harmonic content, it is not possible to model harmonics in programs such as Siemens PTI PSS®E. The two parameters *Vd1* (J+24) and *Vd2* (J+25) represent the voltage below which the PEL is linearly reduced (below *Vd1*) until it all goes to zero (below *Vd2*). Parameter J+132 determined how much of the original PEL recovers once voltage recovers about *Vd2*. These parameters are set to 0.7, 0.5 and 0.8, respectively. That is, it is assumed that below 70% voltage the PEL starts to drop off, and below 50% voltage all of the PEL shuts down. Furthermore, only 80% of the PEL recovers. These numbers are based on observations in the US [1] from laboratory tests and other sources that most power electronic based loads do shunt down somewhere between 0.7 to 0.5 pu voltage, and some small percentage will remain shut down and not turn back on until turned on again by the user.

The ZIP Load Model:

The static load parameters (J+26 to J+36) are explained by the equations shown in Appendix A. This is a simple ZIP model used to represent all remaining loads as a combination of constant current, impedance and constant power loads.

The 3-phase Motor Models (Motor A, B and C):

All the remaining tens of parameters are associated with the four motor models – Motor A, B, C and D. First let us consider the parameters for Motors A, B and C. These three (3) motor models are actually identical in terms of the actual motor model, they are simply the standard model of a 3-phase induction motor (CIM6BL in Siemens PTI PSS®E)[11], with the addition of under-voltage protection. Therefore, parameters J+37 to J+56, which defined Motor A, are repeated three times for these motors. The first of these twenty (20) parameters defines the motor type and thus is always set to 3 (3-phase). The next seven of the twenty parameters are the electrical parameters of the motor model. These are identical for all three motor models (Motor A, B, C) and are the NERC default parameters[12], which are used in North America. Given that these motors represent an aggregated representation of various load components, this is probably as reasonable as any representation. Figure 3 shows the calculated torque-speed characteristic of these generic aggregated motor model parameters[13]. The characteristic is typical of what are called design type A (and B) motors in North America under the National Electrical Manufacturers Association (NEMA)

---

[11] In the other major commercial software platforms, such as GE PSLF™, the 3-phase motors are modeled using a slightly different motor model called *MOTORW*, initially developed by GE. This results in some subtle differences between the model across platforms.

[12] https://www.nerc.com/comm/PC/LoadModelingTaskForceDL/Default%20Data%20Set%20-%20Motor%20A%20B%20C%20Only%20-%20PSSE%20CMLD%20Model.xlsx

[13] The motor A, B, C parameters used here are the same parameters as those used in North America; the torque speed curves are shown, however, calculated for a 50 Hz base frequency.

designations. As can be seen these have a high breakdown torque and a medium/high to normal starting torque. They are most typically used in machine tools, fans, pumps and most such applications. Thus, it is a fairly generic set of parameters and this is why it is used in the US for these aggregated motor models. The further difference between the parameters between Motor A, B and C are the motor under-voltage protection parameters (J+47 to J+56 for Motor A) and the inertia and load torque (J+45 and J+46 for Motor A). Motor A has a low inertia and assumed constant mechanical torque, which is to represent onerous mechanical loads. Motor B has a relatively high inertia and a speed-squared mechanical torque characteristic, indicative of fans. Motor C has again a low inertia with a speed-squared mechanical torque characteristic, assumed to be more typical of pumping loads.
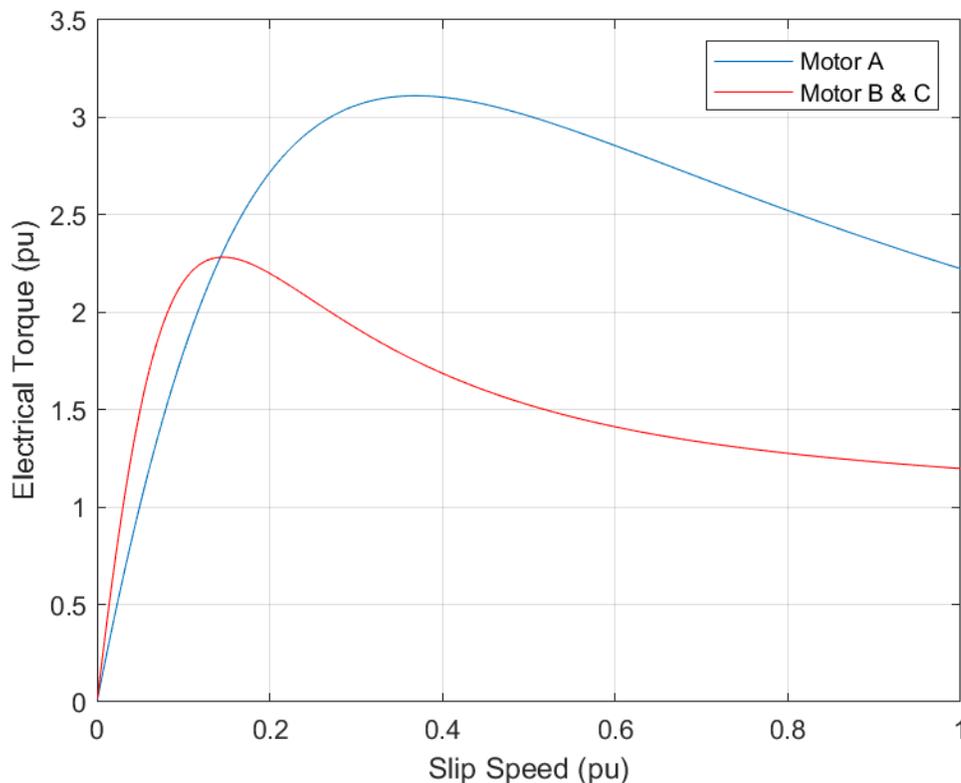
Figure 3: Torque-speed characteristic of the Motor A, B and C motor models.

Each of the three 3-phase motor models have two sets of under-voltage trips settings, which are supposed to emulate under-voltage tripping of large commercial/industrial motors due to actual under-voltage relays [4], and/or contactor drop out. These two sets of parameters are parameters J+47 to J+56 (for Motor A, and duplicate for the others). The values of these trip settings have been set to the default values presented used in the US and publicly discussed within WECC and NERC[14]. We have, however, made one small modification for now, namely disabling the tripping of Motors B and C, by setting *Ftr1B = Ftr2b =*

---

[14] https://www.nerc.com/comm/PC/LoadModelingTaskForceDL/Default%20Data%20Set%20-%20Motor%20A%20B%20C%20Only%20-%20PSSE%20CMLD%20Model.xlsx

Ftr1C = Ftr2C = 0. The trip settings should be briefly explained. The functionality of the trip settings is identical for all three motors. There are two sets of settings for each motor:

- Vtr1A – Under-voltage trip setting 1 (pu)
- Ttr1A – Under-voltage trip time 1 (s)
- Ftr1A – the fraction of the motor that trips for trip setting 1
- Vrc1A – the voltage above which the motor recloses back-in (pu)
- Trc1A – reclose time (s)
- and then a similar set for setting 2

Since these are "aggregated" motor models by setting a value for *Ftr*** only a fraction of the motor can be tripped. If this fraction is set to 0, nothing trips, if it is set to 1 all the corresponding motor component trips.

These trip setting should be reviewed with AEMO to ensure they agree with these assumptions, or if they have better aggregated numbers.

The 1-phase Motor Model (Motor D):

The remaining are all associated with the performance model of the single-phase induction motor model built specifically to represent residential a/c compressor motors used in residential a/c units in the US. These parameters are primarily based on an average of what was derived from extensive laboratory testing of residential a/c units [2], and more recent refinements discussed in the WECC and NERC load modeling task forces. As such, these parameters should not be changed unless the user is absolutely certain that they have better information.

In the case of AEMO the vast majority of a/c load is on the inverter-based high-efficiency systems, which are almost non-existent in the US, and only just starting to be introduced into the US market. The main reason for this is the comparative cost of electricity. Electricity in the US is between ½ to ¼ of the cost of electricity in Australia, with South Australia being the most expensive and Tasmania the least. As such, the higher cost of the inverter-based high-efficiency a/c units is, and has been for perhaps decades, justifiable in Australia given the cost saving in electricity consumption over the life of the unit.

Given the above fact, the percentage of Motor D in the AEMO load models is very low, between 3 to 6%. This is based on AEMOs estimated of what appliances, e.g. refrigeration, some older a/c units, etc. might exist in the Australian system. The vast majority of a/c load has been modeled in the PEL component of the load, since that is the closest load characteristic to an inverter-base a/c.

With all of the above said, the parameters for the CMLD model used here are shown in Appendix A, and the default instantiation of the model is shown below in Table 4.

Table 4: Default instantiation of the CMLDZNU2 model with the parameters used in this report.

```
// Generic
<Zone Number>  'USRLOD'  *  'CMLDZNU2'  12 3  2  133  27  146  48  0  0
-0.8    0     0.04     0.04     0.75     0.08
1    1    1     0.9     1.1
0.00625    1.0     1.02     30     5
0    0     <FmA>     <FmB>     <FmC>
<FmD>     <Fel>    1     0.7     0.5
1    1     <ConstI>    2     <ConstZ>     0
1     <ConstI>    2     <ConstZ>    -1
3    0.75     0.04     1.8     0.12     0.104
0.095     0.0021     0.1     0     0.65
0.1     0.2     0.1     99999     0.5
0.02     0.75     0.65     0.1
3    0.75     0.03     1.8     0.19     0.14
0.2     0.0026     0.5     2     0.55
0.02     0     0.65     0.05     0.5
0.025     0     0.6     0.05
3    0.75     0.03     1.8     0.19     0.14
0.2     0.0026     0.1     2     0.58
0.03     0     0.68     0.05     0.53
0.03     0     0.62     0.1
0.03     0.3     0.025     0.1
1     0.98     0.45     0.1     0.1
 0.0   0.0   1.0   6.0   2.0   12.0   3.2   11.0   2.5   0.86
0.2     0.95     1.0     -3.3     0.5
0.4     0.6     0.52     15     0.7     1.9
0.1     0.5     0.02     0.1     9999     0.8     /Default Settings
```

4.3   Future Load Model Components

Presently, EPRI has proposed a new load model component to better capture the response of inverter-based motor loads, e.g. variable frequency drives (VFD) used in commercial and industrial loads [7]. The model builds a simple refinement, on top of the PEL model structure, to introduce effectively a washout time constant into the model. What this does is that upon a large voltage depression the P and Q of the load drops and then recovers as governed by the washout time constant. While in steady-state and for small voltage fluctuations the load behaves essentially as a constant P/Q load. This behavior better emulates the actual observed behavior of VFD based motor loads, as tested in the laboratory. The current PEL model in the CMLD is slightly pessimistic, when compared to this new proposed model, for capturing the behavior of inverter-connected motor loads.

This newly proposed model has not yet been implemented by the commercial software vendors to be added to the CMLD model. Also, it should be noted that at least one commercial software vendor has already made CMLD a modular format model (i.e. the user can define standard global load component models, and then have single line instantiations of the model at buses simply to designate the appropriate components). Both these enhancements, once available in Siemens PTI PSS®E, will offer more flexibility for composite load modeling in the future. For example, if in the future better information can be ascertained on the amount of VFD based loads in large industrial and commercial loads in Australia, this new component model can be used for those. Certainly, in the US there

is a large move toward VFD motors by large industrials, due to the significant gain in efficiency.

4.4   Testing the Model in the AEMO System

With the explanations provided in the previous subsections, the CMLDZNU2 model was used to populate one of the summer cases with the final files produced being:

> Power Flow Case: *20180104-203047-SubTrans-5digit-SystemSnapshot_NewZones_042419.sav*

> Dynamics Case: *20180104-203047-SubTrans-5digit-SystemSnapshot_WithCMLD_042419.dyr*

The *Cnv_NEM_Loads_v2.py* file (supplied by AEMO) is still used to convert all remaining loads (Zone 1 and 88) to the AEMO static load models and perform some other necessary tasks before initialization.

Thus, of the 1698 loads in the case, 1210 were converted to the CMLD model and the remaining ones (as explained previously those in Zone 1 and 88) remained as static-load models.

With these changes made two simulations cases were run:

- Simulating a 100 ms, 3-phase fault on the radial EHV line emanating from the generator on bus 44504 (in QLD) and tripping the line (and thus also generator[15]), with the existing base case and existing AEMO load model (i.e. all loads throughout the system using the default static-load model that AEMO currently uses).
- Performing the same simulation above, but this time using the newly developed CMLD load model throughout the entire system (1210 loads converted to CMLD).

The results are shown below in Figure 4 and Figure 5. What is plotted is the voltage at an EHV bus close to an adjacent generator (46501), at an EHV bus further away with a near-by off-line generator (46481), an EHV bus not directly connected to either load or generation (45230) and an EHV bus directly serving load (45750).

Three things can be observed:

- With CMLD, the unrealistic voltage spikes down and up at fault inception and clearing disappear from the voltage traces and thus the dip and recovery in voltage looks more realistic and comparable to what one might expect in real life for positive sequence voltage.
- With CMLD, the voltage recovery immediately after fault clearing is significantly more sluggish, as opposed to snapping back up with the existing static-load models.
- Though perhaps a little hard to tell, it does appear that the system is ever so slightly less damped with the CMLD load model.

All these observations are actually as would be expected, and we believe make the simulation results appear more realistic.

One item to note is that upon initialization of the case a hand full (seven to be exact) of the more than 1000 CMLD models return a suspect initial condition. However, the movement

---

[15] **Note:** in this simulation, as a result of the generator trip, system frequency declines. However, the focus here is on load modeling, and so we have only shown voltage traces and only for the first few seconds.

in the DSTATES is in the third decimal point (i.e. 1E-4). Nonetheless, it is clear from the simulations that the model has a clean and flat not disturbance run.
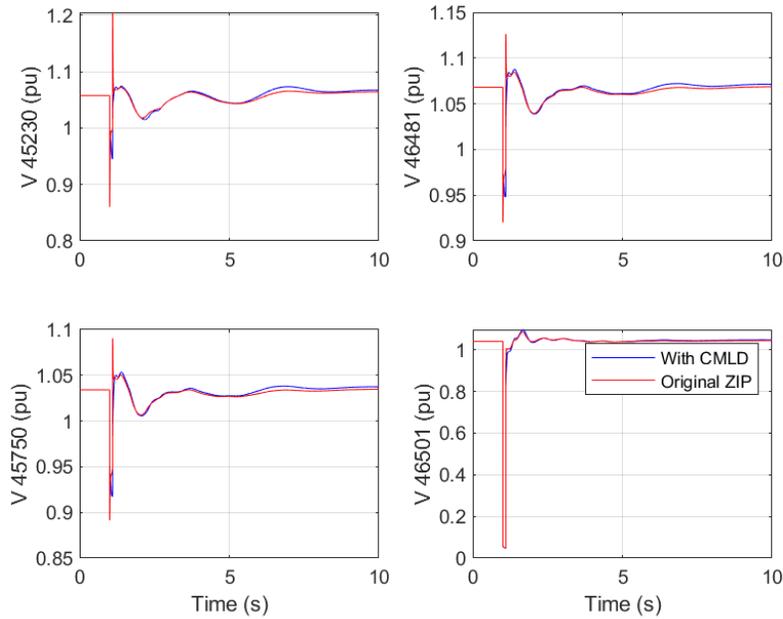
Figure 4: Comparison of simulation results with and without the CMLD load model on the AEMO system.
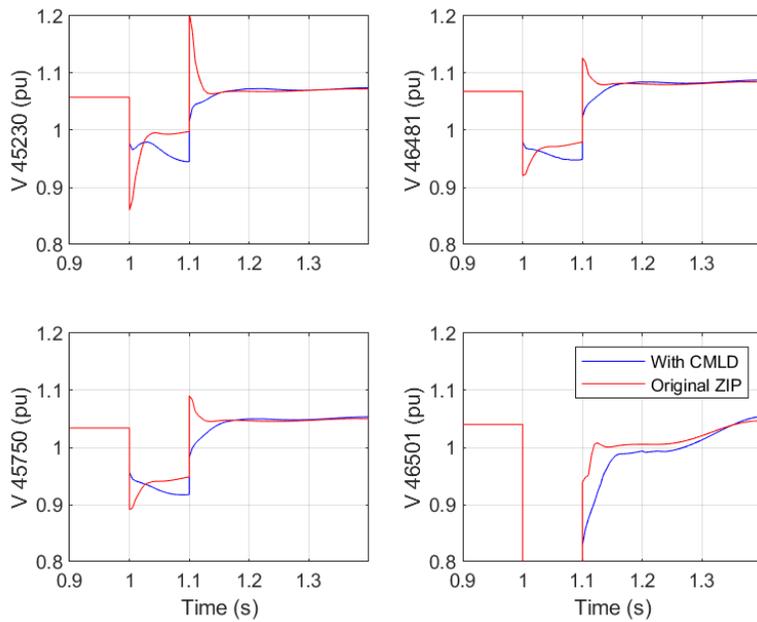
Figure 5: Comparison of simulation results with and without the CMLD load model on the AEMO system – zoomed in version of the plots.

21

5.   Simulations of Events on Distribution Feeders

AEMO provided PEACE® with a number of recoded disturbance events at the ends of three (3) distribution feeders in Queensland. From these we choose several events that were relatively balanced, since severely unbalanced events cannot be faithfully simulated in a positive-sequence simulation platform such as Siemens PTI PSS®E. The feeders are Brendale 11A (primarily residential), Brendale 14B (primarily commercial), and Currimundi (primarily residential). The events that were chosen to be analyzed were:

- Brendale 11A:
    - Event 1 – 1/4/18
    - Event 2 – 2/16/18
    - Event 3 – 5/1/18
    - Event 4 – 6/19/18
- Brendale 14B:
    - Event 1 – 10/21/18
- Currimundi:
    - Event 1 – 2/16/18
    - Event 2 – 11/17/18

Since all these recordings were on a single feeder, it made more sense to analyze these events by employing the so-called playback technique. That is, we set up a simple single machine + load system, and then used the playback function in Siemens PTI PSS®E to play the "positive-sequence" component of the recorded 3-phase voltage into the CMLD model and then to compare the measured and simulated 3-phase load P (MW) and Q (MVar). This is depicted in Figure 6.

11 kV

Small Impedance
j0.01 pu

Playback
Voltage Source

Load Model
(CMLD or AEMO's
original ZIP model)
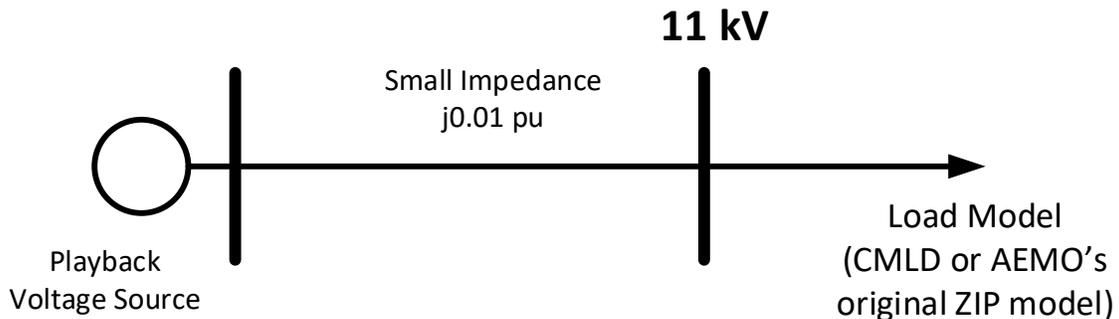
Figure 6: Simple playback model for simulating distribution feeder events.

A few cases were at first simulated in both GE PSLF™ and Siemens PTI PSS®E, to ensure consistent results, since recently in North America there has been much work done in groups such as WECC LMTF and NERC LMTF to try to ensure that the CMLD model gives consistent results across the platforms. As such, some updates have been made to the CMLD, particularly in Siemens PTI PSS®E. A comparison is thus shown, in Figure 7 , for one of the cases. This shows clearly that the results are consistent between the two platforms. This issue aside, let us now look at the results from all the cases. The remainder of the simulations shown in the report are all in Siemens PTI PSS®E Version 34.5.1.
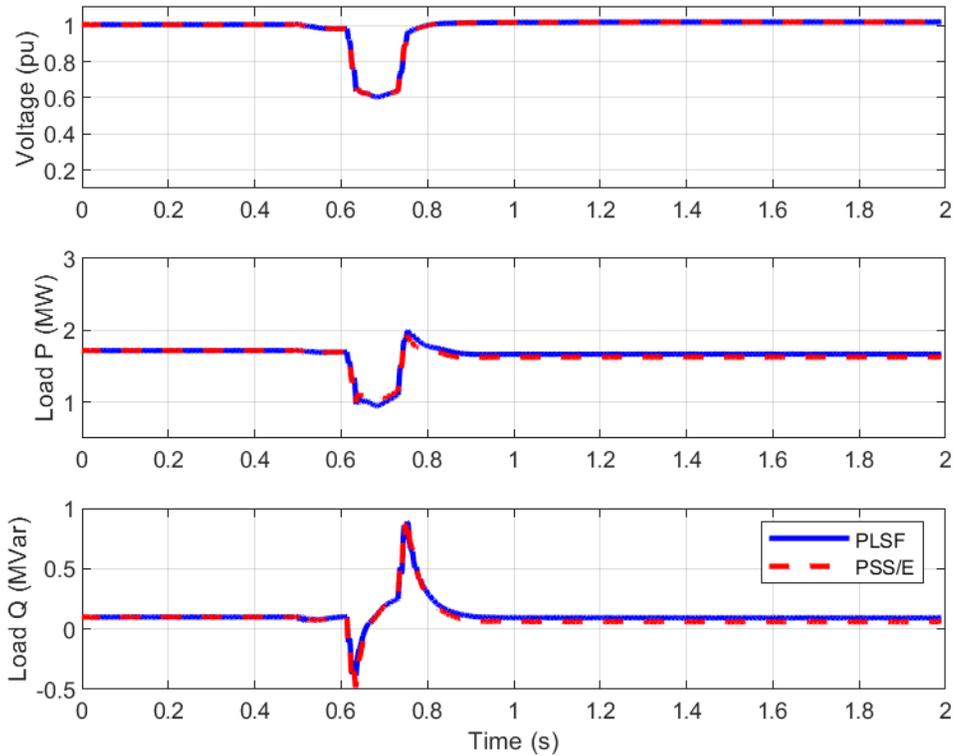
Figure 7: Comparison of a playback simulation for one of the Brendale events (Event 1) in GE PSLF™ and Siemens PTI PSS®E. As can be seen both programs give the same result.

5.1   Brendale 11A Feeder

For the Brendale 11A Feeder we looked at four (4) events in 2018. AEMO indicated that this is primarily a residential feeder in a suburb north-west of Brisbane, Queensland. The events occurred on 1/4/18 (Event 1), 2/16/18 (Event 2), 5/1/18 (Event 3) and 6/19/18 (Event 4). A number of simulations were performed.

First, all four events were simulated using the "average" CMLD model for the entire state of Queensland – that is the CMLD model in section 4, and the fractions of the load components being those in Table 1 for Events 1, 2 and 3, and Table 2 for Event 4. It is recognized that Event 3 is not a summer event, but rather a mid-autumn event, but we used the summer numbers since only the summer and winter numbers were available. The results, in comparison to the current AEMO static ZIP load model, are shown in Figure 8.

Next, all four events were simulated this time using the "residential" composition numbers derived in AEMO's composition spreadsheet, for Queensland, for a summer evening (for Events 1, 2 and 3) and a winter evening (for Event 4).
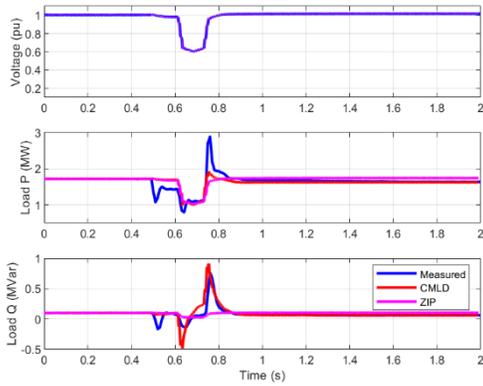
a) Event 1
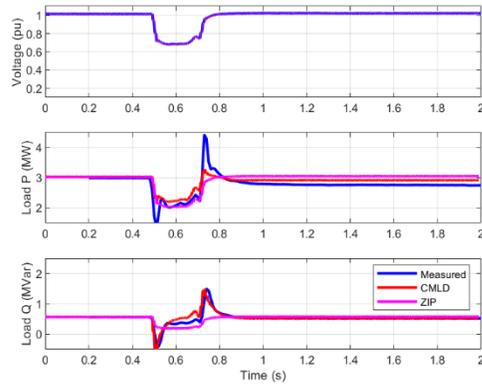
b) Event 2
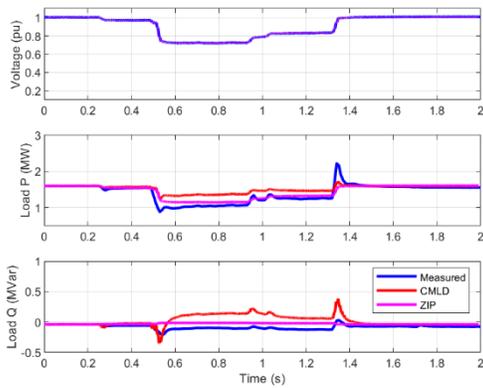
c) Event 3
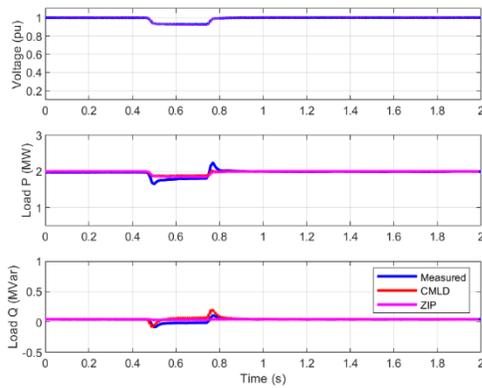
d) Event 4

Figure 8: Comparison of a playback simulation for Events 1 to 4 on the Brendale 11A feeder, using the "average" Queensland CMLD composition numbers.

a) Event 1
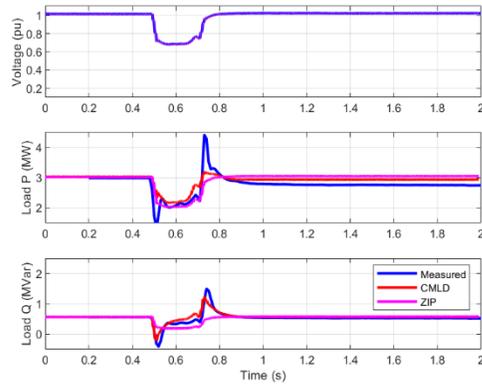
b) Event 2
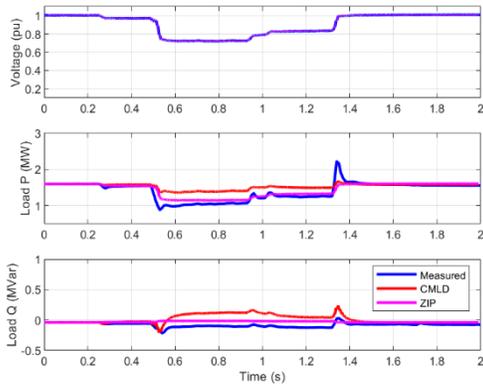
c) Event 3

d) Event 4

Figure 9: Comparison of a playback simulation for Events 1 to 4 on the Brendale 11A feeder, using the "residential" Queensland CMLD composition numbers.

Perusing the result in Figure 8 and Figure 9 the following observations can be made:

1. The CMLD model in general does a better job of capturing the actual measured response of the load, particularly for the reactive power (Q) response.
2. Events 1, 2 and 3 are certainly more interesting, with greater voltage dips.
3. There is not a tremendous difference between the simulation results for these events when using either the "average" or "residential" load compositions for the respective seasons.
4. It can be seen in a few of the cases that there appears to be some load loss during and immediately after the fault that is not well captured by either model.

On the last note, such load loss cannot be captured at all with the existing AEMO static ZIP load model. However, CMLD can capture this both with the trip settings of the power-electronic load and those of the 3-phase motors. Thus, tweaking these values for Event 3, the result shown in Figure 10 is achieved. This is still not perfect, but is much closer now to the measured response. In all the cases with CMLD the reactive power (Q) response much more closely matches the measured response, while the spike in real power response immediately after fault clearing is not as pronounced in the simulated CMLD model. The

existing static ZIP load model, presently used by AEMO, does not capture any of the spikes in P and Q, nor the apparent load loss.
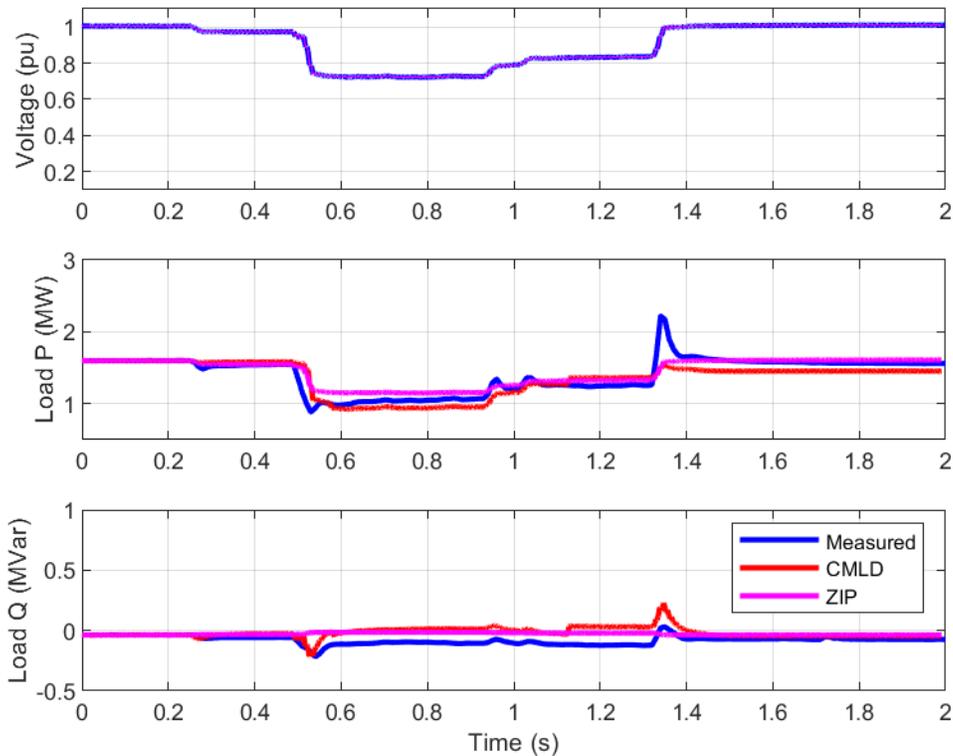
Figure 10: Comparison of a playback simulation for Event 3 on the Brendale 11A feeder, using the "residential" Queensland CMLD composition numbers, and adjusting some of the parameters of the model related to tripping of the electronic and 3-phase motor loads.

5.2   Brendale 14B Feeder

For the Brendale 14B feeder, which based on AEMO's information is primarily a commercial feeder, one of the more onerous, yet close to balanced events, was simulated (Event 1 – 10/21/18). The results are shown in Figure 11, Figure 12 and Figure 13. Again, it can be seen that:

1. The CMLD model in general does a better job of capturing the actual measured response of the load, particularly for the reactive power (Q) response.
2. There is not a tremendous difference between the simulation results for these events when using either the "average" or "residential" load compositions for the respective seasons.
3. Tweaking some of the parameters related to the power electronic and 3-phase motor trip settings, a closer match can be obtained between the measured and simulated response for the CMLD model[16].

---

[16] Throughout this report and the effort hear, the motor trip settings have only been engaged and tweaked on the Motor A model. The trip settings on Motor B and C have been disabled. The reason for this was three fold (i) to minimize the number of parameters to be tweaked, (ii) for lack of better information on the Motor

4. The measured real power (P) spike immediately after fault clearing is not as pronounced in the simulated CMLD model response.
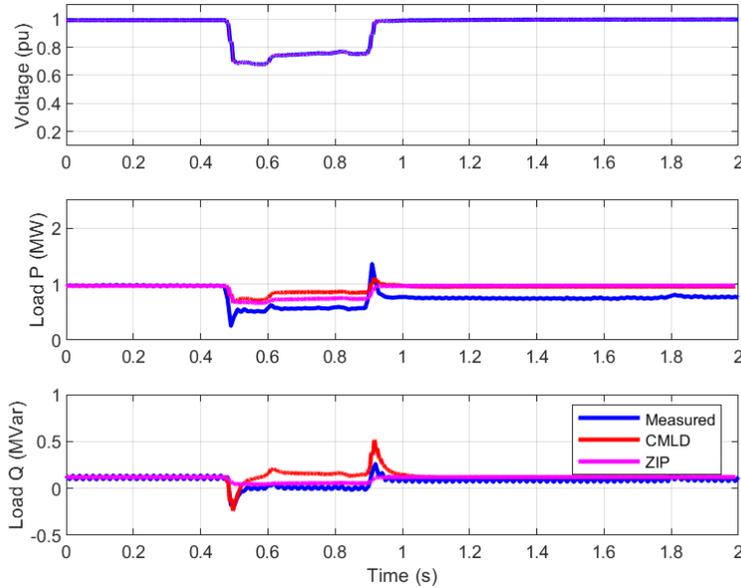
Figure 11: Comparison of a playback simulation for Event 1 on the Brendale 14B feeder, using the "average" Queensland CMLD composition numbers.
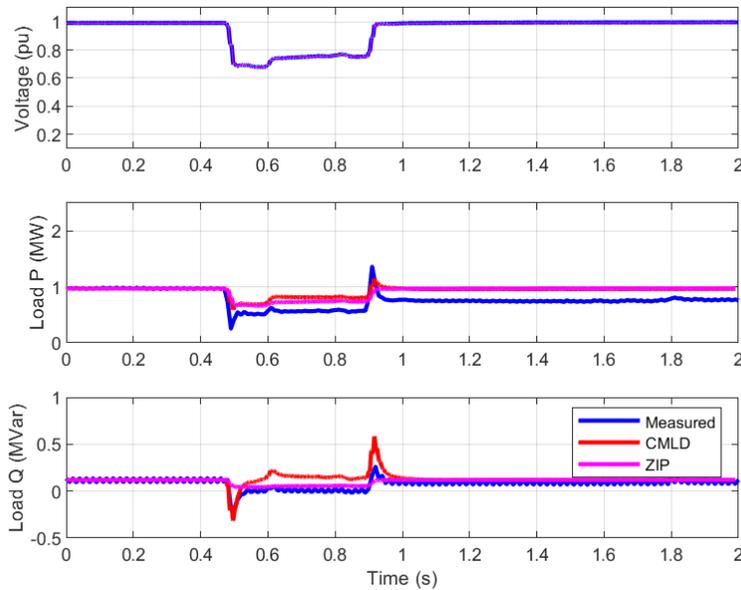
Figure 12: Comparison of a playback simulation for Event 1 on the Brendale 14B feeder, using the "commercial" Queensland CMLD composition numbers.

B and C trip settings that may be applicable in Australia – the default NERC values may be used if better information specific to Australia is not presently available, and (iii) in order to be conservative presently with regards to the amount of motor load that trips during severe faults.
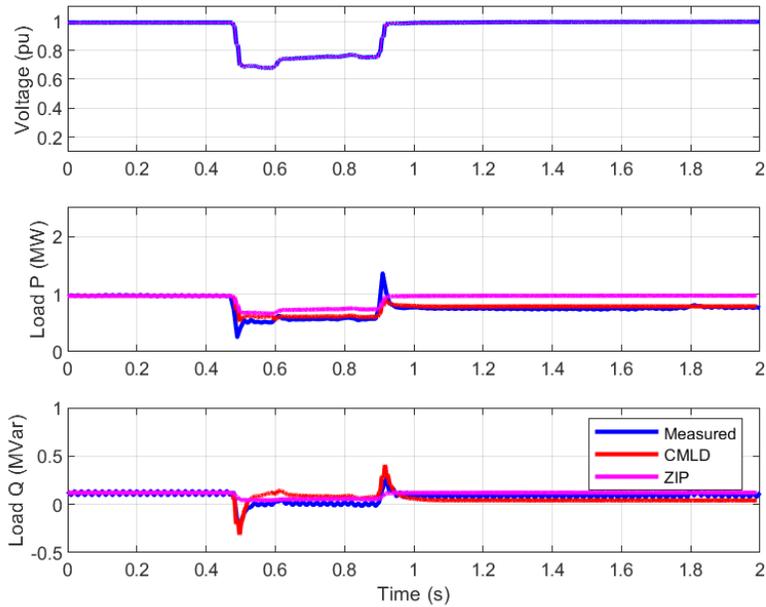
Figure 13: Comparison of a playback simulation for Event 1 on the Brendale 14B feeder, using the "commercial" Queensland CMLD composition numbers, and adjusting some of the parameters of the model related to tripping of the electronic and 3-phase motor loads.

5.3   Currimundi Feeder

For the Currimundi feeder, which based on AEMO's information is also primarily a residential feeder, two events were simulated (Event 1 – 2/16/18 and Event 2 – 11/17/18). The results are shown in Figure 14, Figure 15 and Figure 16. Again, the same general observations as for the Brendale feeders can be made, that the CMLD model in general does a better job of capturing the actual measured response of the load, particularly for the reactive power (Q) response.
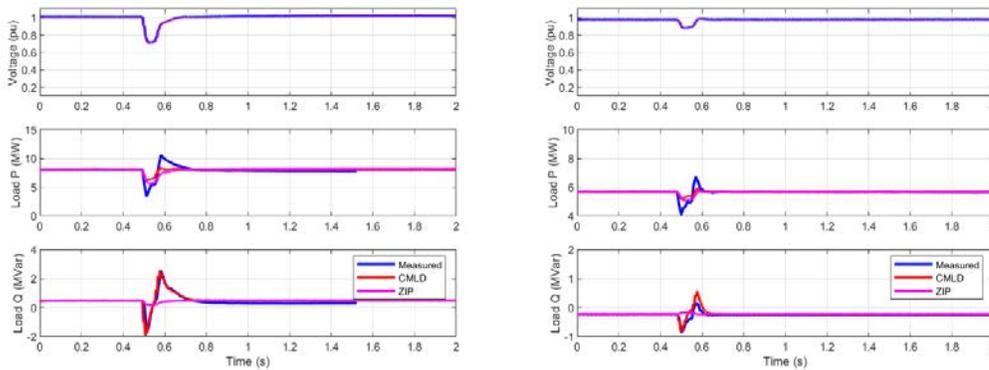
a) **Event 1**   b) **Event 2**

Figure 14: Comparison of a playback simulation for Events 1 and 2 on the Currimundi feeder, using the "average" Queensland CMLD composition numbers.
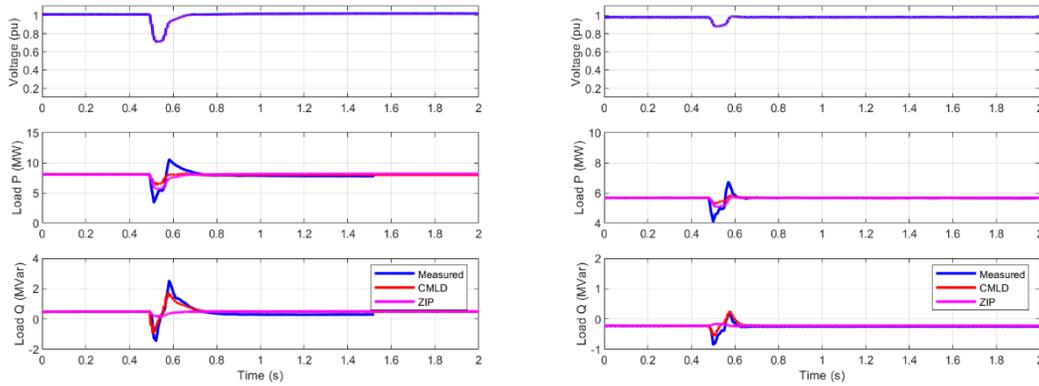
a) Event 1   b) Event 2

Figure 15: Comparison of a playback simulation for Events 1 and 2 on the Currimundi feeder, using the "residential" Queensland CMLD composition numbers.
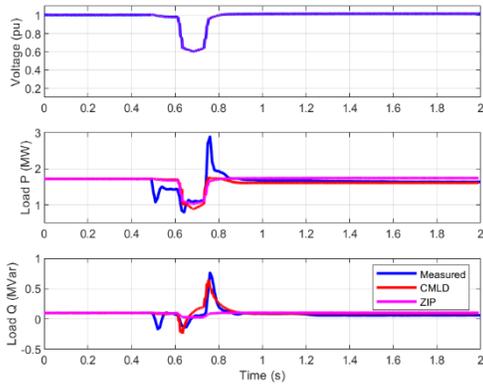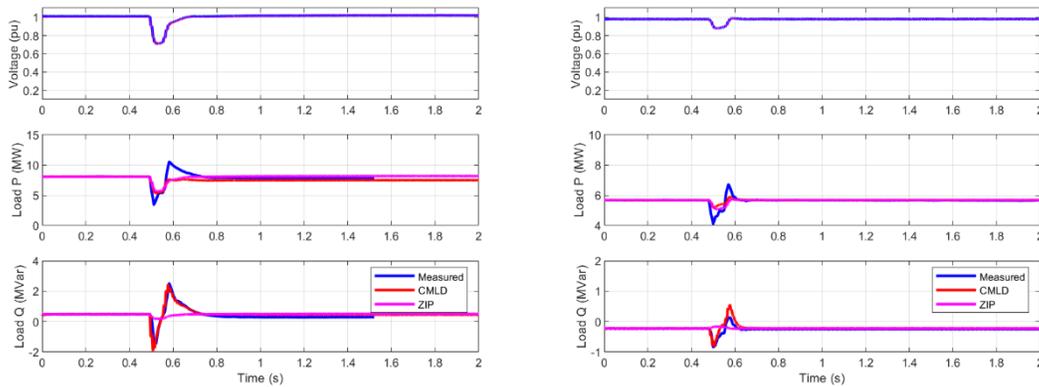

a) Event 1   b) Event 2

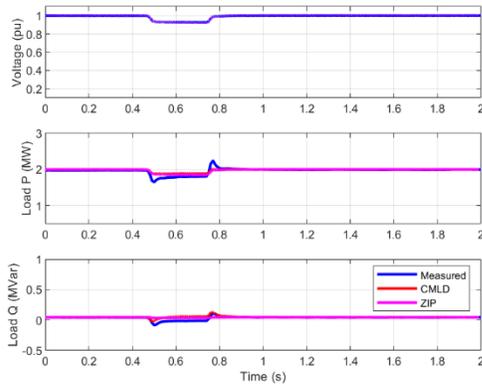**Figure 16: Comparison of a playback simulation for Events 1 and 2 on the Currimundi feeder, using the "average" Queensland CMLD composition numbers, and adjusting some of the parameters of the model related to tripping of the electronic and 3-phase motor loads.**

5.4   Conclusions and Key Takeaways

From the analysis of the feeder level measurements, and attempting to simulate them using both the proposed new CMLD model and the existing AEMO static ZIP load model, it can be seen that the existing ZIP load model only shows voltage dependence during the fault. Thus, it does a rather poor job of matching either the P or Q response of the load. Furthermore, it cannot capture the apparent loss of load seen in some of the events.

In contrast, the CMLD load model captures quite well the Q response of the load, and captures the general trend of the P response of the load, however, the spike in the real power (P) immediately after clearing of the fault, is not as pronounced in simulation as it is in the measurements. Furthermore, by tweaking the tripping points of the electronic and 3-phase motor loads, the apparent loss of load in many of the events, due to the voltage dip, can be emulated with the CMLD model.

In all the cases it is evident that there is some load tripping for the more severe voltage dips (i.e. greater than 20%). In these cases, it was found that by changing the power electronic load trip settings to *Vd1* = 0.8, *Vd2* = 0.6 and *Ferst* = 0.5, and in some cases slightly increasing the amount of Motor A tripping, a better match was achieved in the MW response of the load.

To further investigate the issue with the mismatch between the CMLD simulations and the measured load real power (P) response at fault inception and clearing, one of the events was simulated in a series of sensitivity runs, while trying to tweak various parameters. Figure 17 shows one of the results of these sensitivity runs, where it can be seen now that the P response matches quite well, while the Q response significantly over-estimates the spikes in reactive power upon inception and clearing of the voltage-dip. In this case the amount of Motor A was increased to 45%, and Motor B to 20%, with the power electronic load reduced to accommodate. This does not necessarily mean that this particular feeder and event has so much more motor load content, since the Q response now is far too excessive. What it illustrates is the effect of the motors on the P and Q response. Thus, we might be able to get a much better match of both P and Q, if:

1. The motor load content was refined, and
2. The motor load electrical parameters were tuned to the particular feeder response.

There may also be other underlying factors, such as the unbalance in the actual events. Finally, even if one was to get a near perfect match for this one case, that is only one event on one feeder in the entire system. Thus, it would not be warranted to use that model across the entire system.
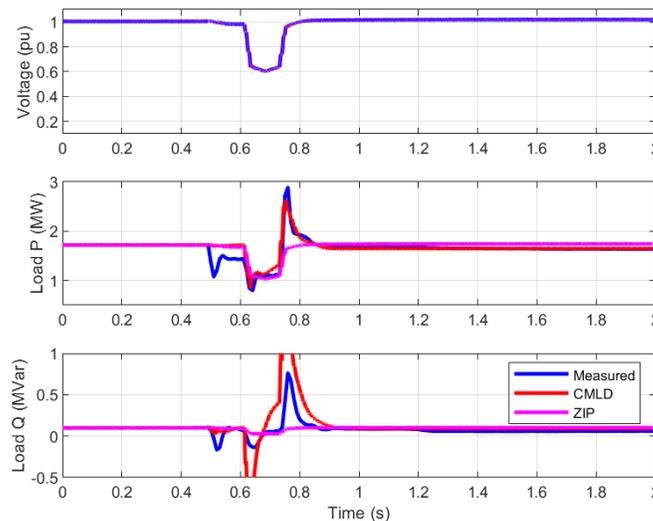
Figure 17: Comparison of a playback simulation for Events 1, for the Brendale 11A feeder, with a significantly adjusted composition of the load – for example, the Motor A component was drastically increased to 45%.

6.   Simulations of Large System Events

AEMO provided PEACE® with a few recoded disturbance events that have occurred at the extra high-voltage (EHV) transmission level, and for which AEMO had phasor measurement unit (PMU) recordings on several transmission nodes across the system. From these we chose, after discussion with AEMO, two of the events that were significant and for which AEMO had the most information and has separately composed both Siemens PTI PSS®E base cases and PSCAD cases. The chosen events are:

- **Event 1:** the 12/9/18 Victorian event, which was a line-to-ground fault, presumably at Rowville Transmission Station, which was then cleared in 54 ms with both of the Hazelwood to Rowville 220 kV lines tripping.
- **Event 2:** the 4/17/19 South Australian event, which occurred due to a bush-fire that resulted in the fault and tripping of the Torrens Island to Magill 275 kV line.

For event 2, based on discussions with AEMO, we assumed that the fault occurred at the Magill end and that it was cleared in 5-cycles (100 ms). In both cases, obviously the exact fault impedance is not known, so iterative simulations were performed with varying fault impedance in order to get as close as possible on the nadir of the voltage (during the fault) at the majority of the recorded EHV buses.

6.1   The Victorian Event – Event 1

Starting with the snapshots provide by AEMO (*.raw and *.dyr) the following steps were taken:
1. One case was simulated with the existing AEMO load model, i.e. static ZIP load models per the AEMO provided *Cnv_NEM_Loads_v2.py*.
2. One case was simulated with the newly developed CMLD model as presented in section 4. Namely:
    a. Placing all the loads in the new zones described in section 4.1.
    b. Applying the CMLDZNU2 model to each of the zones as described in section 4.1, and all remaining loads staying as static loads. Thus, the initial CMLD parameters are those in appendix A, and the load component percentages are the summer percentages per Table 1 (and Table 3 for power plant auxiliary loads).

The files thus developed are:

Power Flow model: *20181209-020017-SubTrans-5digit-SystemSnapshot_New_Load_Zones.sav*

Dynamics model:

> *20181209-020017-SubTrans-5digit-SystemSnapshot_New_Load_Zones.dy*r (with CMLD)

> *20181209-020017-SubTrans-5digit-SystemSnapshot.dyr* (with AEMO's ZIP load model)

The previously provided user-written model DLL library (*dsusr_34-5.dll*) was also used.

The results of the simulations are shown in Figure 18 through Figure 23. These need to be explained as follows:

1. First consider Figure 18 and Figure 19. These show the comparison between the measured voltages at key EHV buses (light blue, orange and yellow for the three

phases), for the event, and simulations using the existing AEMO ZIP load model (red), and the newly developed CMLD model (bright blue). It can be seen that the ZIP model cases the voltages snap back up almost immediately following the fault, while the CMLD cases the voltage recovery is somewhat slower and smoother recovery, similar to the actual voltage measurements. There are three key subtleties to be noted:

    a. The voltage recovery with the ZIP load model cases is significantly faster than the actual measurements.

    b. The voltage recovery with the CMLD load model is in many of the cases slightly more delayed than the measurements, i.e. more pessimistic.

    c. The PMU measurements are at a rate of one data point per cycle (20 ms intervals). This is the best resolution available. However, such resolution is perhaps inadequate to truly capture the nuances of the voltage dip and recovery during and immediately after the fault. This is because the fault itself lasted no more than about 2.5 cycles. Also, note that at Rowville, where the fault appears to have occurred, the PMU apparently shut-down for roughly ½ second from the time of the fault inception, so there is no useful data available at that bus. If available, digital fault recorder (DFR) type data may prove more useful in the future.

2. Now consider Figure 20 and Figure 21. In these cases, we simulated the event assuming a bolted 3-phase fault was the initiating event at Rowville station. Clearly, the actual event was not a bolted 3-phase fault – such faults (3-phase fault to ground) are extremely rare. None-the-less, we wanted to see the comparison between the two load models for such a simulation, since 3-phase faults are often simulated in transmission planning studies. It can be seen that the CMLD model now results in a very significant fault-induced delayed voltage recovery. The voltage on most of the buses takes roughly 1 second to recover back to its pre-fault values. This delayed voltage recovery is due to the stalling of the Motor D component of the CMLD model. In the case of the load composition work performed by AEMO (see Table 1 and Table 2) the percentage of Motor D[17] is quite small throughout Australia, between 3 to 6% of the load. Thus, the delayed voltage recovery is not very slow, as compared to what has been actually observed in North America at some locations where it can take the voltage many seconds to tens of seconds to recover due to massive penetration of Motor D type loads associated with residential air-conditioning. Consider Figure 22 and Figure 23. In this case the same 3-phase fault was simulated, but this time the Motor D component was removed, and moved to the static-load component. Clearly, the fault-induced delayed voltage recovery is no longer apparent. Furthermore, note that as seen from the initial simulations, the fault type (i.e. 3-phase versus emulation of 1-phase fault) and location will also affect whether the Motor D component stalls (*Vstall* being 0.45 pu as set in the model). All this simply points to the importance of future work to better understand the actual penetration of Motor D type loads in the Australian system, and sensitivities that need to be played around the load model. **<u>Important</u>**

---

[17] Motor D represents single-phase, capacitor-start, conventional induction motors for residential and light-commercial loads, particularly in air-conditioning and similar type loads (e.g. refrigeration, heat-pumps, etc.)

Note: another known fact, based on research and development in North America[18], is that the stalling of these so-called Motor D type loads is driven by many factors, some of which cannot be truly captured in a positive-sequence simulation tool such as Siemens PTI PSS®E. For example, the rate at which the voltage drops, the point-on-wave where the fault occurs, the type of mechanical load and the configuration of transformer windings (i.e. Y-Delta etc.) can all influence what the actual motors see at their terminals down at the low voltage levels where these type motors are used, and thus drive if and how the motor stalls. As such, in the end some level of sensitivity analysis is needed when trying to capture the potential for delayed voltage recovery.

---

[18] https://certs.lbl.gov/initiatives/fidvr

Figure 18: Comparison of a simulation to measurement at key EHV buses for the Victorian event – Event 1. Emulated fault with significant fault impedance to try to match nadir of the measured voltages in most of the cases. Default CMLD parameters.
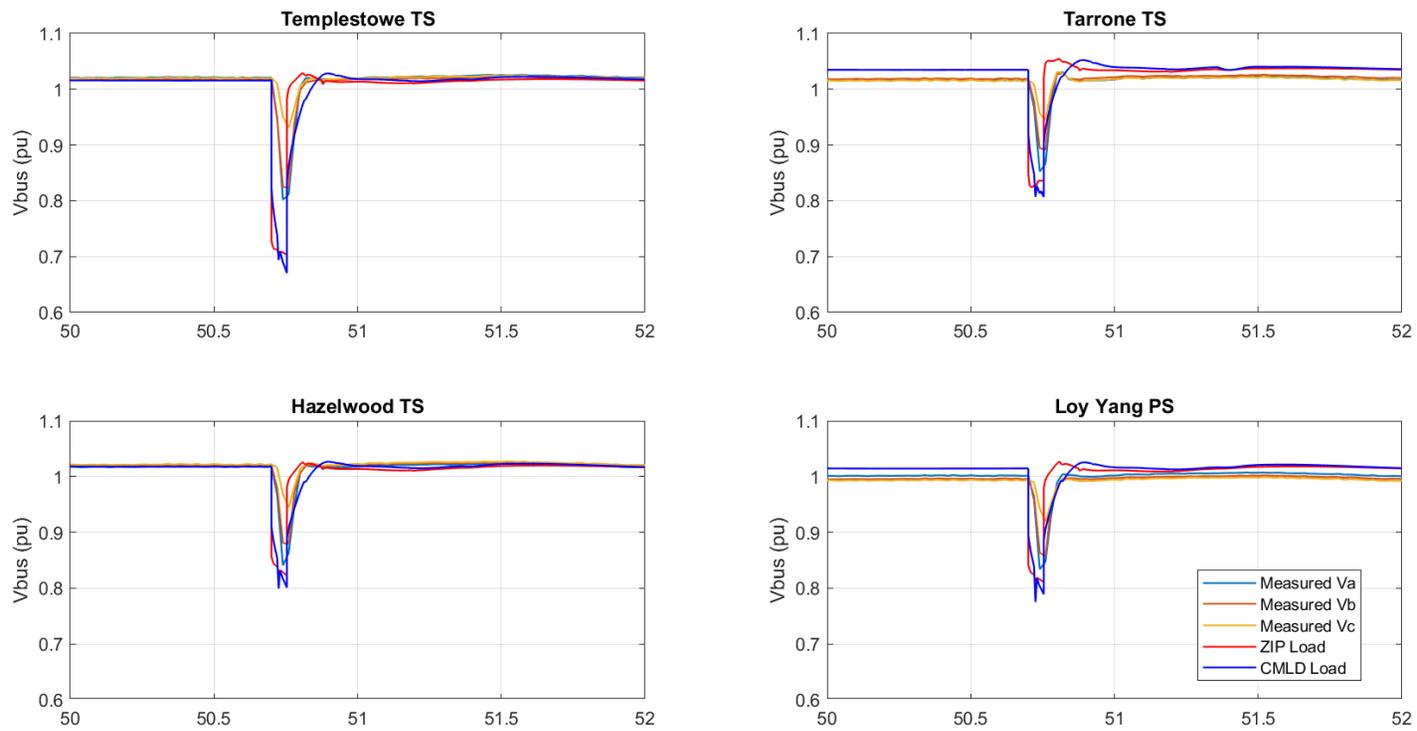
Figure 19: Comparison of a simulation to measurement at key EHV buses for the Victorian event – Event 1. Emulated fault with significant fault impedance to try to match nadir of the measured voltages in most of the cases. Default CMLD parameters.

Figure 20: Comparison of a simulation to measurement at key EHV buses for the Victorian event – Event 1. <u>Simulated a 3-phase bolted fault at Rowville Transmission Station – which is much more severe than the actual event.</u> Default CMLD parameters.

Figure 21: Comparison of a simulation to measurement at key EHV buses for the Victorian event – Event 1. Simulated a 3-phase bolted fault at Rowville Transmission Station – which is much more severe than the actual event. Default CMLD parameters.

Figure 22: Comparison of a simulation to measurement at key EHV buses for the Victorian event – Event 1. <u>Simulated a 3-phase bolted fault at Rowville Transmission Station – which is much more severe than the actual event.</u> Removed Motor D component from CMLD, and moved it to ZIP component. Also, made slight changed to power electronic load trip settings per results in section 5.

Figure 23: Comparison of a simulation to measurement at key EHV buses for the Victorian event – Event 1. <u>Simulated a 3-phase bolted fault at Rowville Transmission Station – which is much more severe than the actual event.</u> Removed Motor D component from CMLD, and moved it to ZIP component. Also, made slight changed to power electronic load trip settings per results in section 5.

6.2   The South Australian Event – Event 2

The same approach was once again taken for developing the models. For the CMLD model the compositions for summer (Table 1) where used, though it is realized that the event occurred during autumn. This is because at this point, we only have composition estimates for summer and winter. So, to be conservative, we assumed the summer numbers.

The files thus developed are:

Power Flow model: OPDMS_STNET_JYU_20190328T164426_20190430T165629_NewZones.sav

Dynamics model:

OPDMS_STNET_JYU_20190328T164426_20190430T165629_CMLD.dyr (with CMLD)

OPDMS_STNET_JYU_20190328T164426_20190430T165629.dyr (with AEMO's ZIP model)

The previously provided user-written model DLL library (dsusr_34-5.dll) was also used.

The results of the simulations are shown in the Figures below. These need to be explained as follows:

1. First consider Figure 24 and Figure 25. These show the comparison between the measured voltages at key EHV buses (light blue), for the event, and simulations using the existing AEMO ZIP load model (red), and the newly developed CMLD model (bright blue). It can be seen that the ZIP model cases the voltages snap back up almost immediately following the fault, and in some cases have a slight overvoltage spike immediately after the fault. The CMLD cases, however, have a voltage recovery that is slower and smoother, and matches quite closely the actual measured system response.

2. Now consider and Figure 26 and Figure 27. In this case the simulation was rerun, this time by adjusting some of the power electronic load trip settings to affect a significant loss of load due to the fault. As such, one can see that in the CMLD case the voltages settle at a slightly higher voltage post-fault, similar to the measured cases. The point here is not that the tweaks in the parameter are necessary the exact and correct adjustments, but rather that the CMLD model can emulate load loss, while the ZIP model cannot. Further adjustments that can emulate load loss are the trip settings of the large 3-phase motor components (Motor A, B and C).

3. Finally, again we simulated the event assuming a bolted 3-phase fault was the initiating event at Magill station. Again, the voltage recovery for the CMLD case is slower than the ZIP model case (Figure 28 and Figure 29), however, this time the significant fault-induced delayed voltage recovery is not seen. This is likely due to two reasons: (i) the percentage of Motor D in South Australia is lower than Victoria, and (ii) the location of the fault is remote enough from the major load pockets that the voltage at the loads does not fall below *Vstall* (0.45 pu) and thus the Motor D components do not stall.
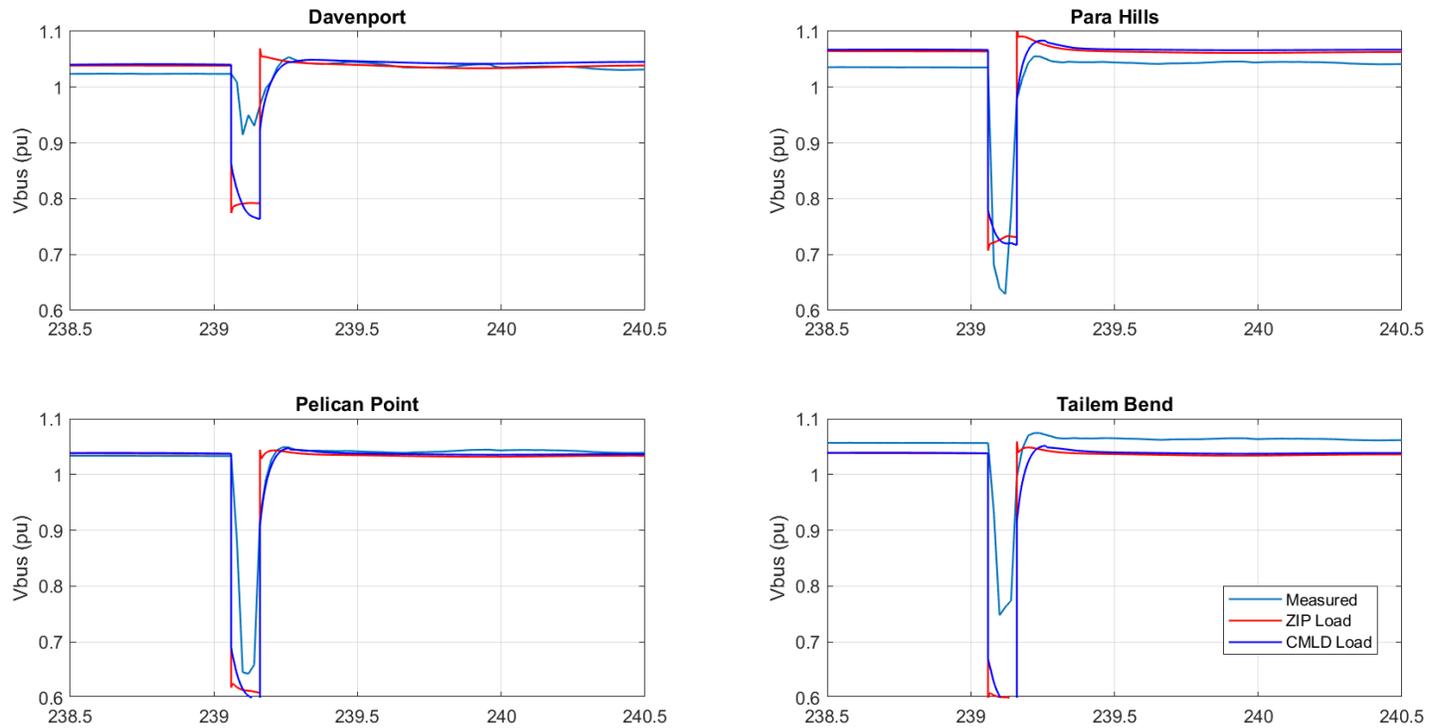
Figure 24: Comparison of a simulation to measurement at key EHV buses for the South Australian event – Event 2. Emulated fault with significant fault impedance to try to match nadir of the measured voltages in most of the cases. Default CMLD parameters.
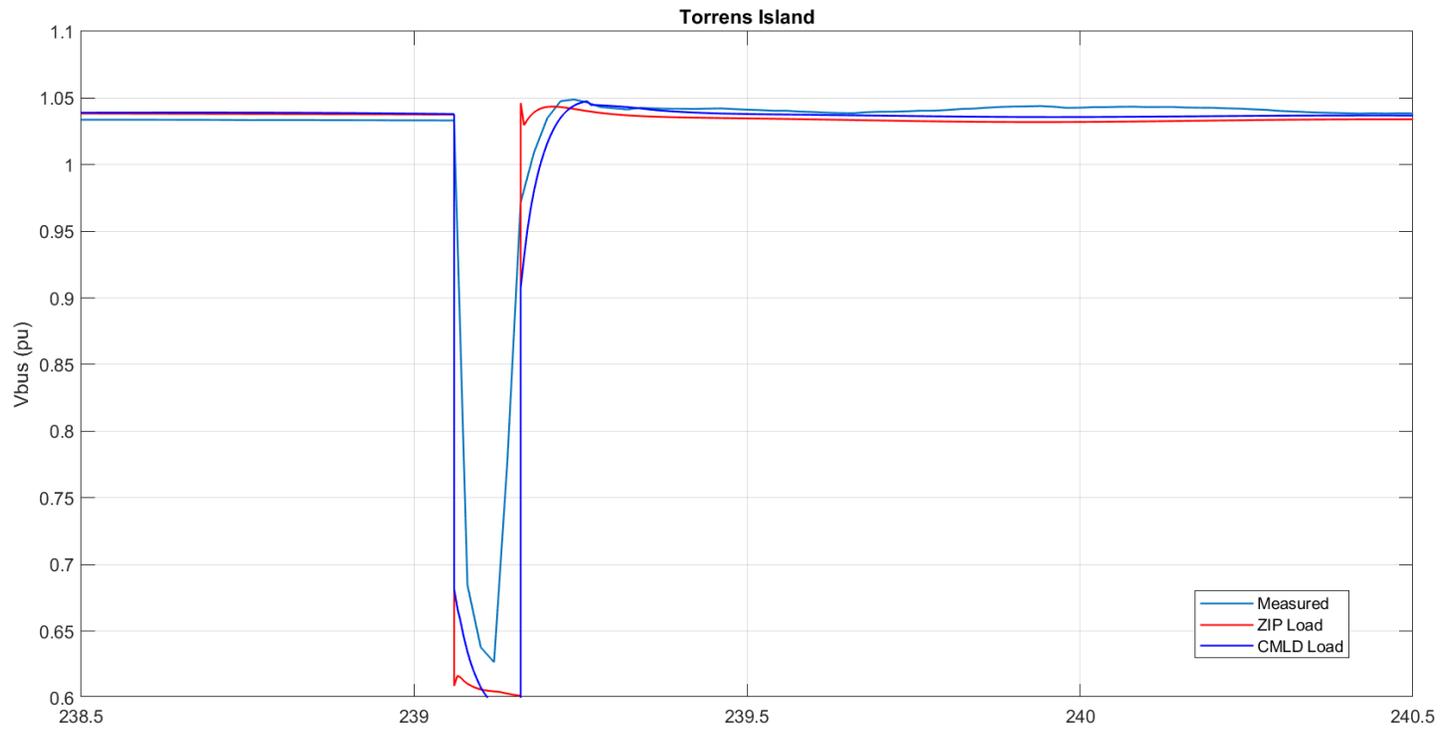
Figure 25: Comparison of a simulation to measurement at key EHV buses for the South Australian event – Event 2. Emulated fault with significant fault impedance to try to match nadir of the measured voltages in most of the cases. Default CMLD parameters.
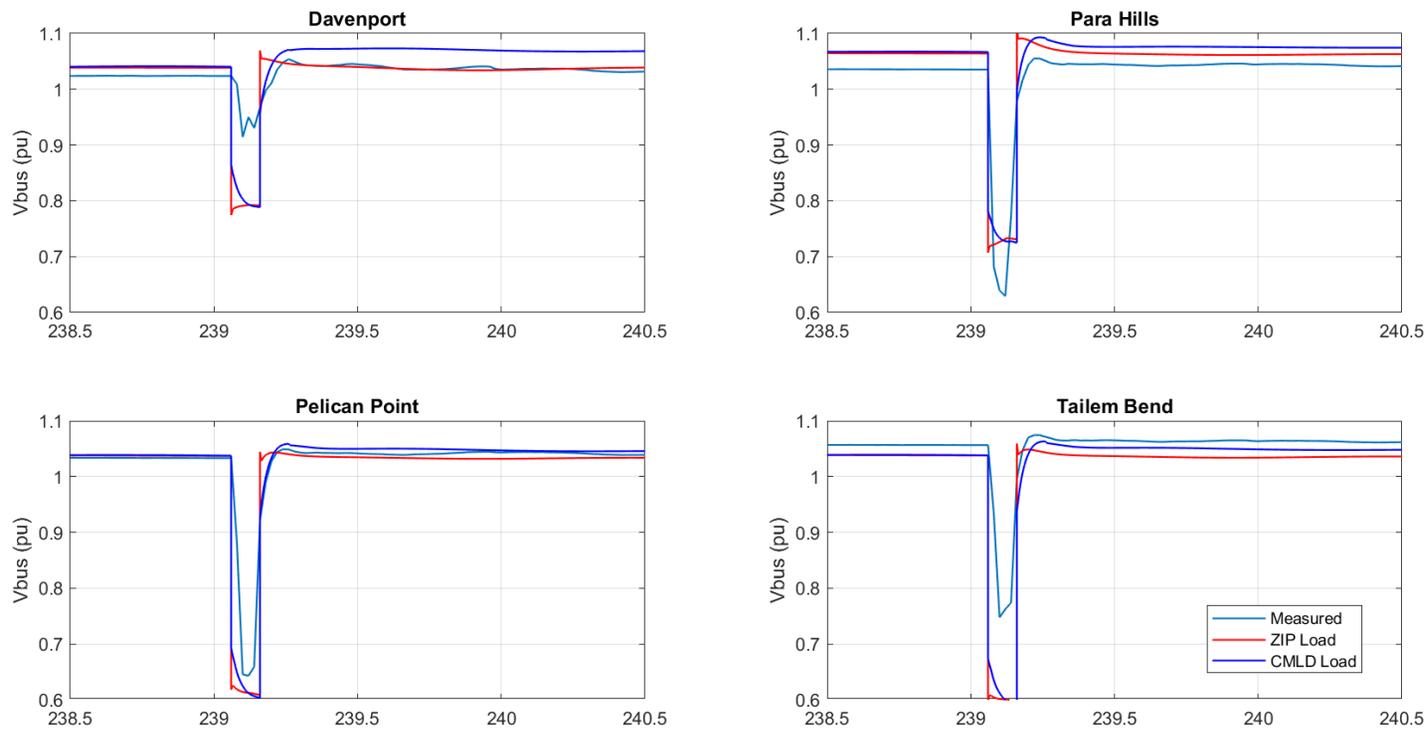
Figure 26: Comparison of a simulation to measurement at key EHV buses for the South Australian event – Event 2. Emulated fault with significant fault impedance to try to match nadir of the measured voltages in most of the cases. Adjusted power electronic load trip settings for CMLD (i.e. *Vd1* = 0.8, *Vd2* = 0.6 and *Ferst* = 0.1).
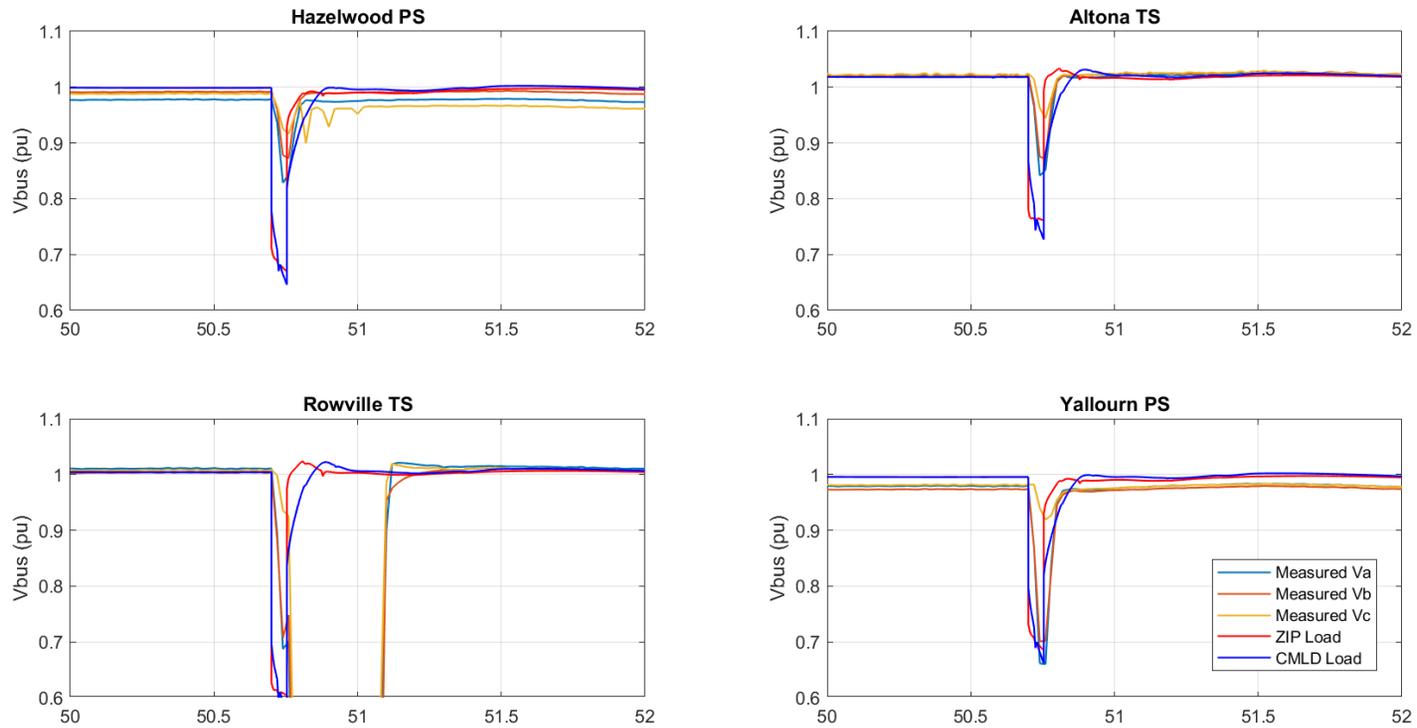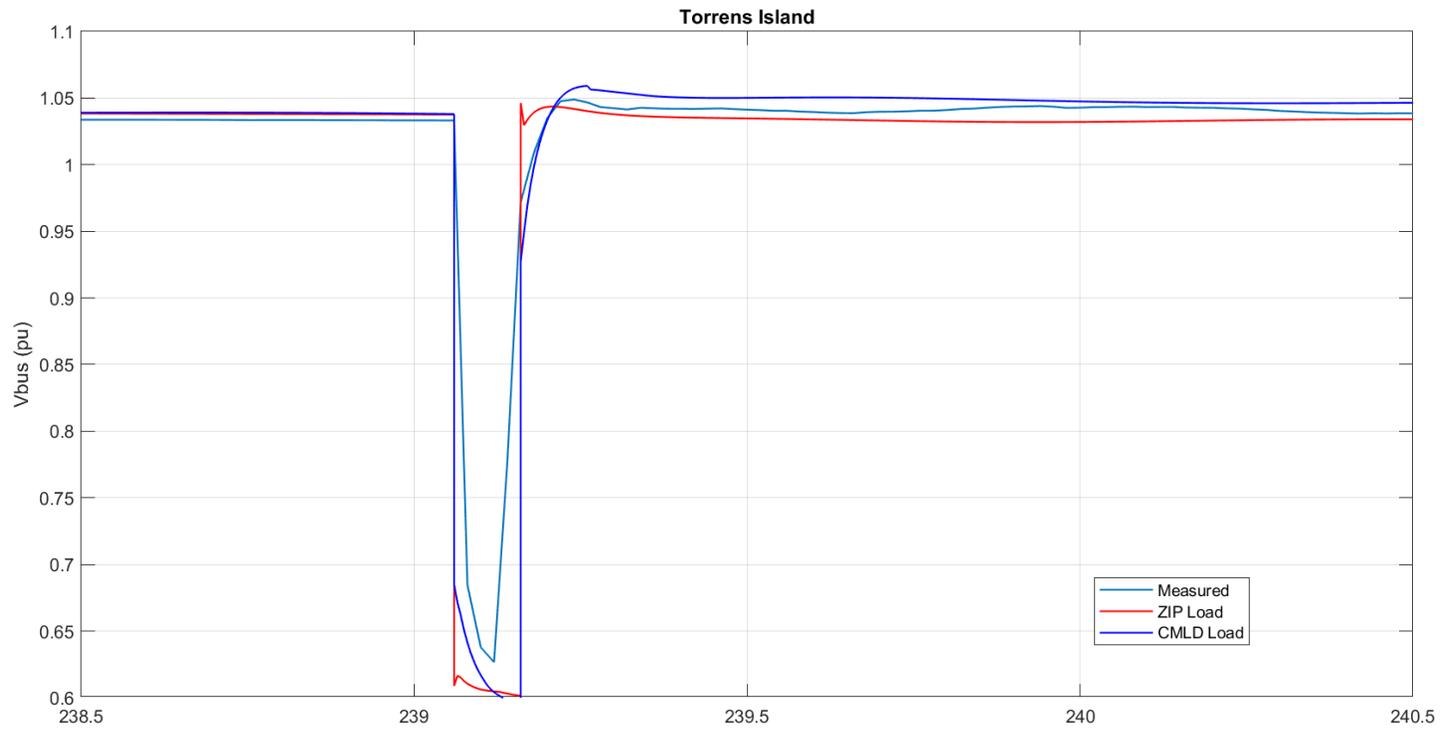
Figure 27: Comparison of a simulation to measurement at key EHV buses for the South Australian event – Event 2. Emulated fault with significant fault impedance to try to match nadir of the measured voltages in most of the cases. Adjusted power electronic load trip settings for CMLD (i.e. *Vd1* = 0.8, *Vd2* = 0.6 and *Ferst* = 0.1).
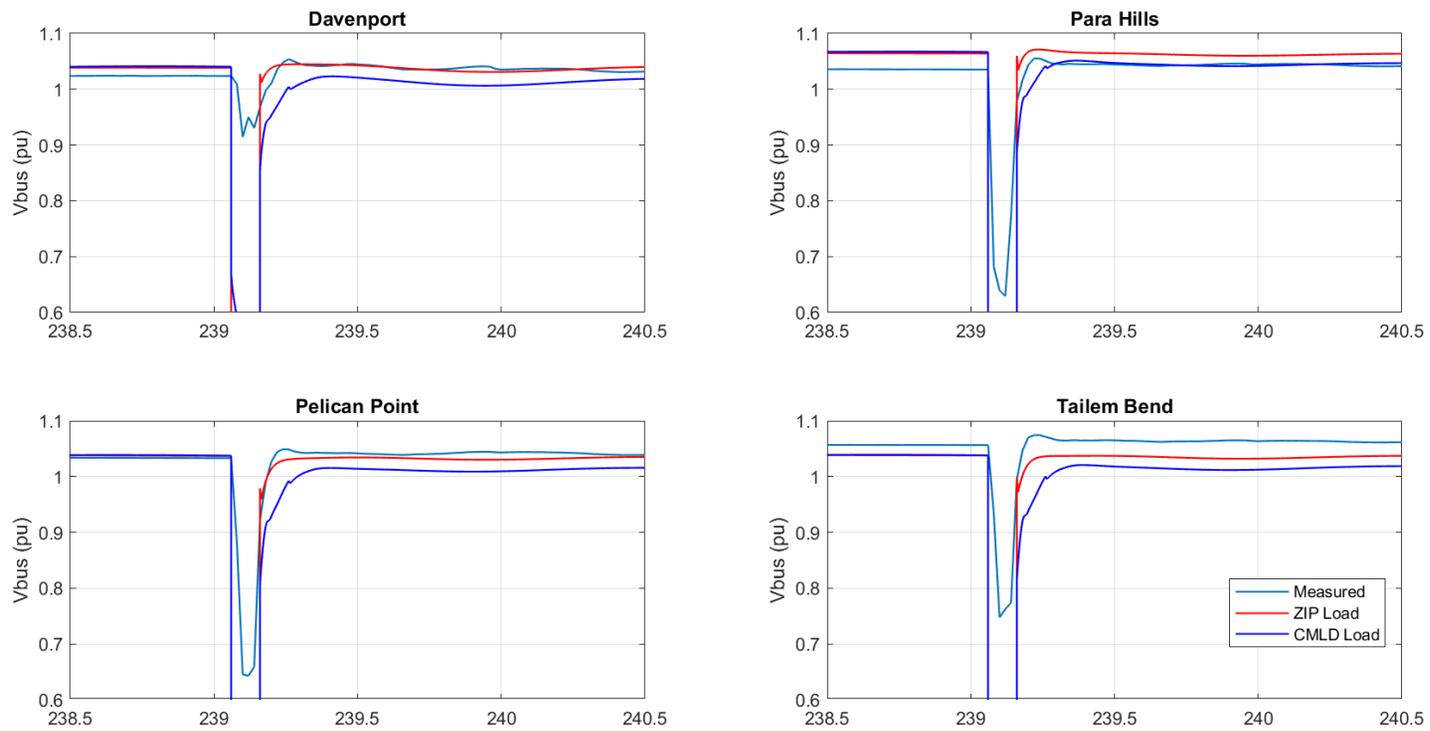
Figure 28: Comparison of a simulation to measurement at key EHV buses for the South Australian event – Event 2. Simulated a 3-phase fault at Magill.

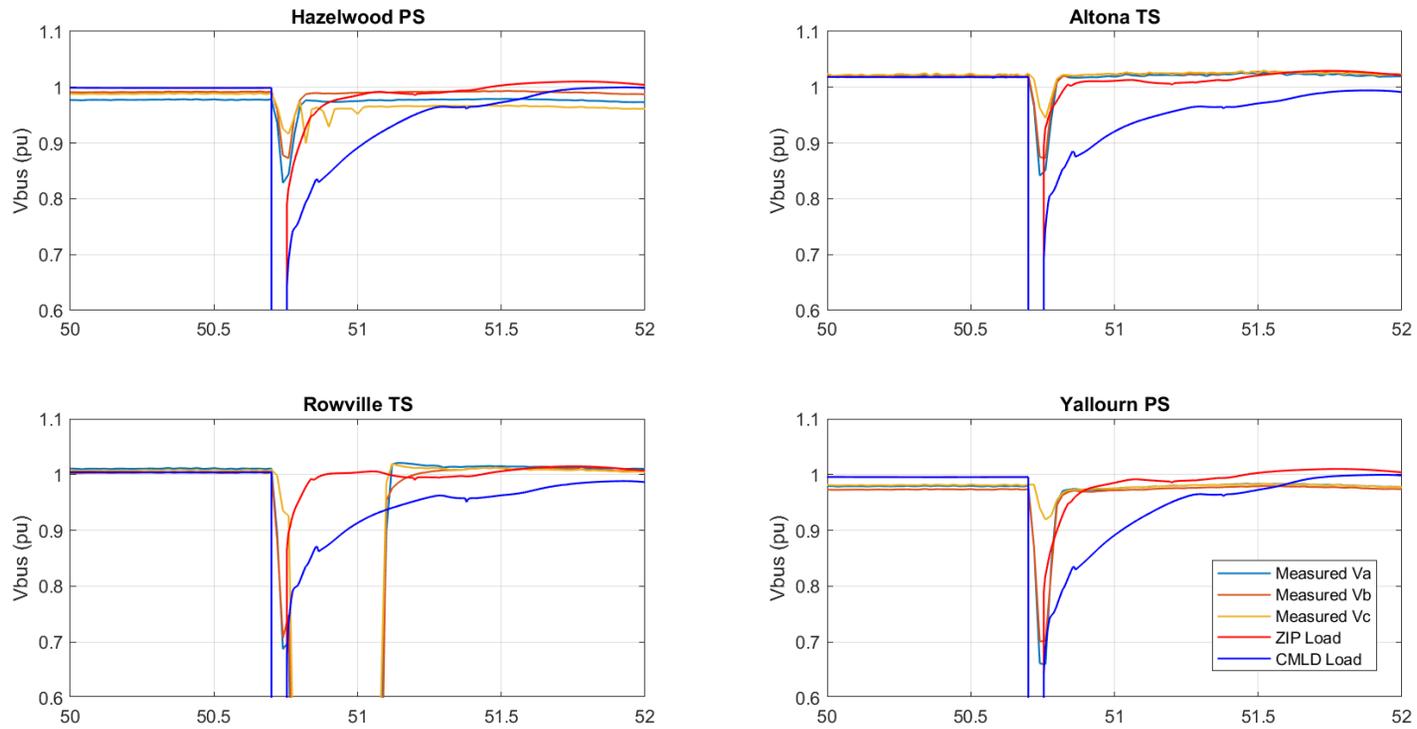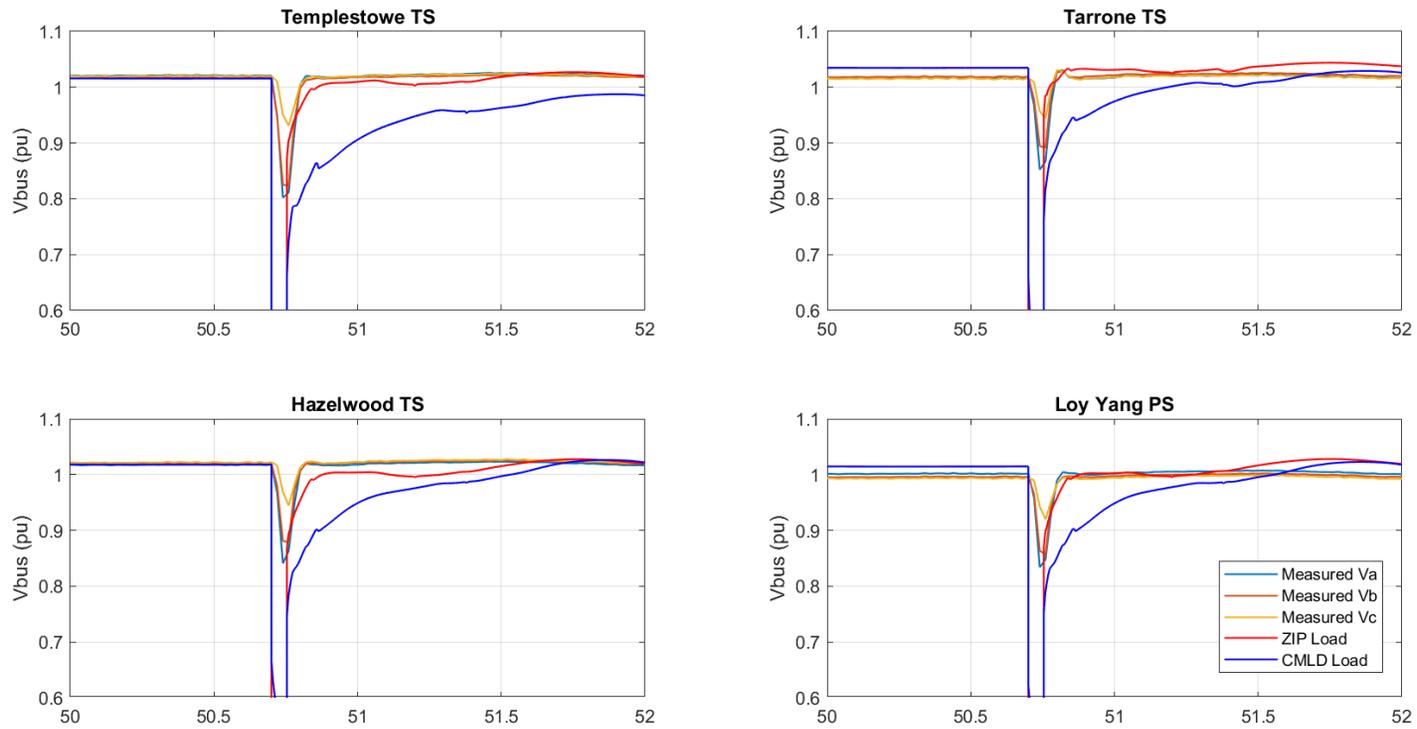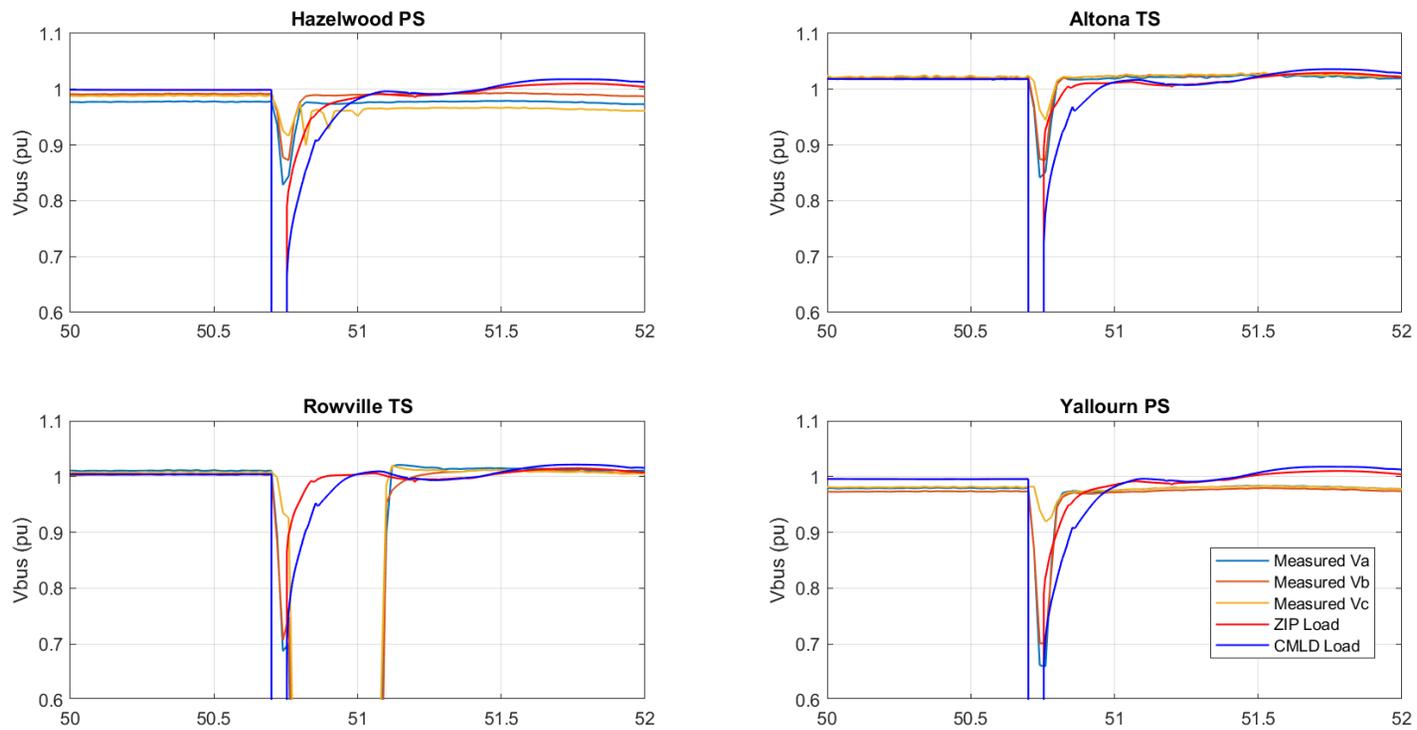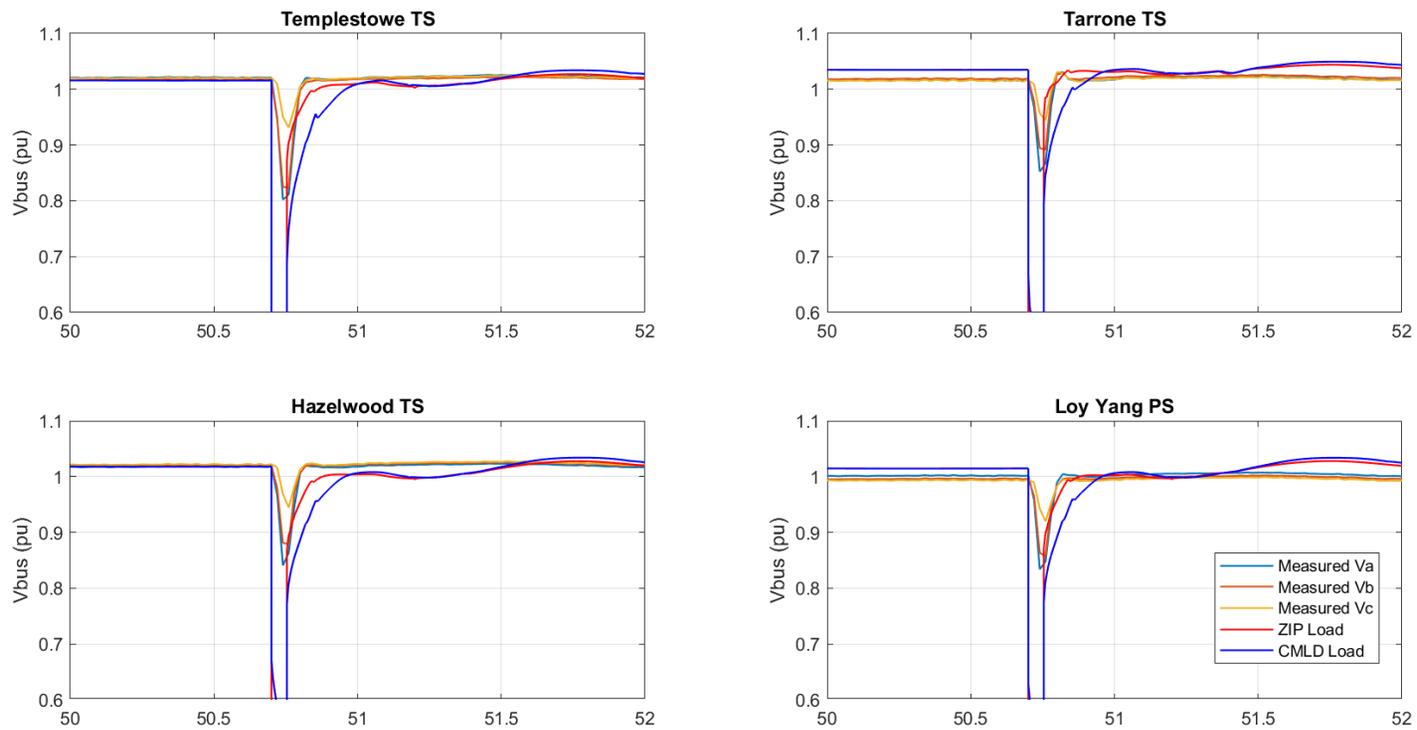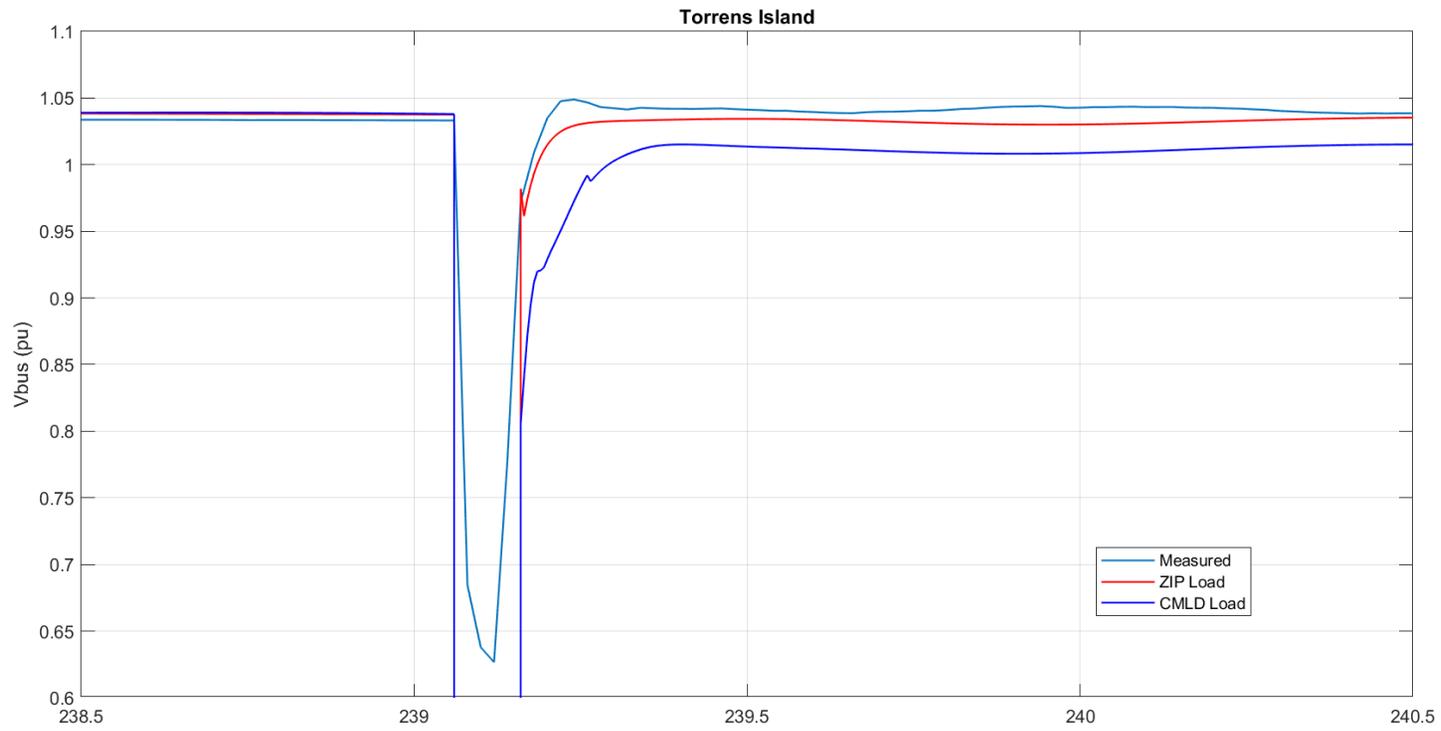**Figure 29: Comparison of a simulation to measurement at key EHV buses for the South Australian event – Event 2. Simulated a 3-phase fault at Magill.**

7.   Including the Distributed Energy Resource Models

The next step in the work was to include the modeling of the distributed energy resource (DER) modeling into the composite load model. The vast majority, if not all, of the DER on the Australian system is presently distributed solar photovoltaic (PV) generation. AEMO thus provided to PEACE® a number of both distribution recorded events, at the Brendale 11A feeder and the Currimundi feeder, as well as a few system wide events, all of which had significant PV on-line. The goal being to use the CMLD model developed and discussed in the previous sections, together with incorporating a model of the DER. To model the DER, the so-called DER_A model recently developed in North America [3] is used here.   Furthermore, present efforts in North America have been focused on incorporating the DER_A model into the CMLD model, as shown in Figure 1, in order to make it one integrated model emulating a single aggregated model of the distribution feeder, the aggregated composite load model, and an aggregated model of the DER on the feeder. This single model incorporating CMLD and DER_A, called *CMLD**DGU2* in Siemens PTI PSS®E, has just as of 6/13/19 been tentatively approved within the WECC MVWG, after a few months of rigorous testing and benchmarking across the four main software platforms in North America within the WECC MVWG, with the testing work being led by EPRI. Thus, this model is only available presently in the commercial software platforms (such as Siemens PTI PSS®E) as a beta version upon request from Siemens PTI. Thus, all the simulation work presented here uses this beta version, requested from Siemens PTI, and provided in version 34.5.1. Therefore, AEMO should note that if any simulations are to be performed with this model the very latest version of Siemens PTI PSS®E should be used, and a beta version of the model requested from Siemens PTI. Given the recent tentative approval of the model, the official release of the model may come out in the next minor release of Siemens PTI PSS®E. It should be noted that the CMLD**U2 model has been approved and available in Siemens PTI PSS®E for some time, as well as the standalone DER_A model. It is only this combination of the two into a single integrated model that has not yet been officially released.

7.1   The DER_A Model

The DER_A model specification can be found publicly on-line on the WECC website [3]. However, for the sake of completeness a very brief and high-level description of the model is given below. The model block diagram is shown in Figure 30. The key features of the model are as follows:

1. This model is intended to emulated the aggregated behavior of a large number of distributed generators in the distribution system.   To this end, many of the parameters do not necessarily translate to an actual physical setting on distributed generation, but are rather an attempt to capture aggregated behavior. For example, the parameters *Vrfrac, vl0, vl1, vh0, vh1, tvl0, tvl1, tvh0* and *tvh1* collectively allow for emulation of partial tripping of the aggregated DER. This is explained in detail in [3].
2. The model (top left-hand part) allows for constant power factor, constant Q-control and voltage control emulation, with asymmetric deadband. The voltage control is simple, and only allows for proportional control.

3. The frequency tripping is modeled with a simple definite time trip setting. If frequency goes below *fl* for more than *tfl* seconds, or goes above *fh* for more than *tfh* seconds, then the entire model will trip.

4. The model allows for modeling ramp-rate limits on the real-power recovery following a fault, or during primary-frequency response, and also models a basic current limit with P/Q priority options.

5. The model can also emulate distributed energy storage (see [3]), but for the purposes of our use here, we are only interested in model PV generation.

6. The model can emulate basic primary-frequency response functionality. For the AEMO case only the downward regulation (i.e. reducing power due to an over-frequency) is used.

A list of the model's parameters, with default values for the AEMO system, is given in Appendix B. The default parameter values were determined in consultation with AEMO staff, and the reasoning behind the chosen values is given in the table.

7.2   The CMLD**DGU2 Model

In Siemens PTI PSS®E (and several other commercial software programs) the CMLD and DER_A models have been available as separate models for some time. They have also been tested and approved in WECC. However, here we are using the CMLD**DGU2 model, which is still only a beta released model in Siemens PTI PSS®E Version 34.5.1. This model incorporates DER_A into the CMLD model (as shown Figure 1) such that the load and DER are all at the end of the aggregated distribution feeder model. The CMLD model within the CMLD**DGU2 model has a slightly different order of parameters for the composite load model piece, and so the list of parameters and the values used here (based on the CMLD and DER_A models in Appendix A and B) are listed in Appendix C.

7.3   Simulating Distribution Feeder Events for Brendale 11A and Currimundi

Per discussions with AEMO, the only feeder events worth considering presently were those that occurred on Brendale 11A and Currimundi, since the PV inverters on Brendale 14 B have certain peculiarities which are presently under consideration. Thus, we selected a suitable event from the Brendale 11A feeder and another from the Currimundi feeder.

The Brendale 11A event occurred on April 12, 2018. Being closer to summer, the summer load compositions from section 6 were used. AEMO estimates that the PV was at a capacity of 31% at the time of the event. There is 2.6 MW of nameplate installed PV on the feeder, thus this means that 806 kW was being generated by the PV prior to the event. The net load prior to the event was 287 kW. Thus, we modelled the case with 1093 kW of load and 806 kW of DER in the power flow case[19]. The model then assigns the CMLD portion to the load and the DER_A portion to the DER. The results of the simulations are shown in Figure 31.

---

[19] In the actual Siemens PTI PSS®E case the load and DER was scaled up by a factor of 100 to avoid numerical issues with the CMLD model when dealing with very small loads, and then for plotting purposes the values are scaled back down. Similar actions were taken for the cases with load modeling only in section 6.
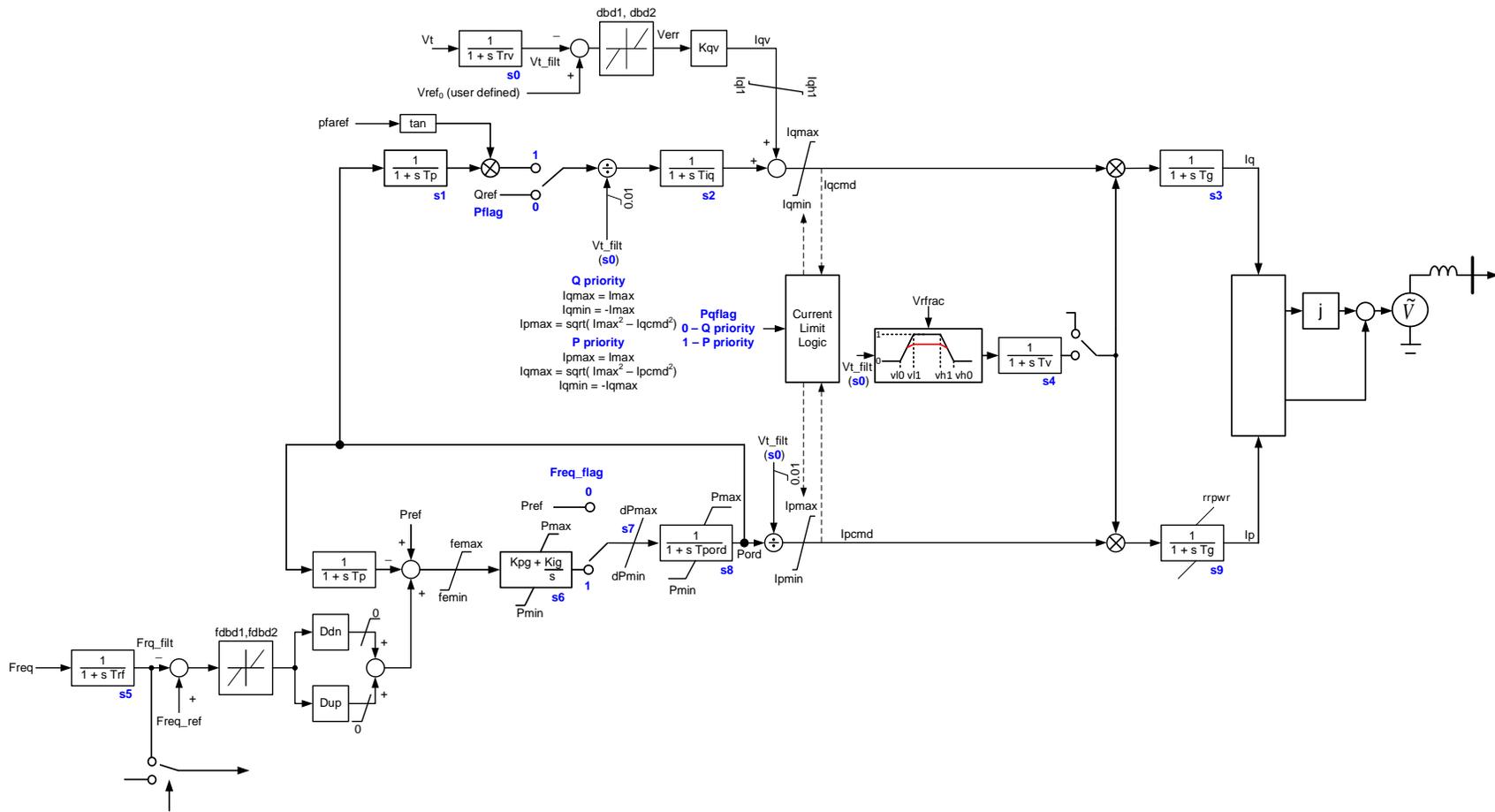
Figure 30: The DER_A model.

The Currimundi event occurred on December 4, 2018. Being in summer, the summer load compositions from section 6 were used. AEMO estimates that the PV was at a capacity of 42% at the time of the event. There is 7.12 MW of nameplate installed PV on the feeder, thus this means that 2990 kW was being generated by the PV prior to the event. The net load prior to the event was 5072 kW. Thus, we modelled the case with 8062 kW of load and 2990 kW of DER in the power flow case. The model then assigns the CMLD portion to the load and the DER_A portion to the DER. The results of the simulations are shown Figure 32.
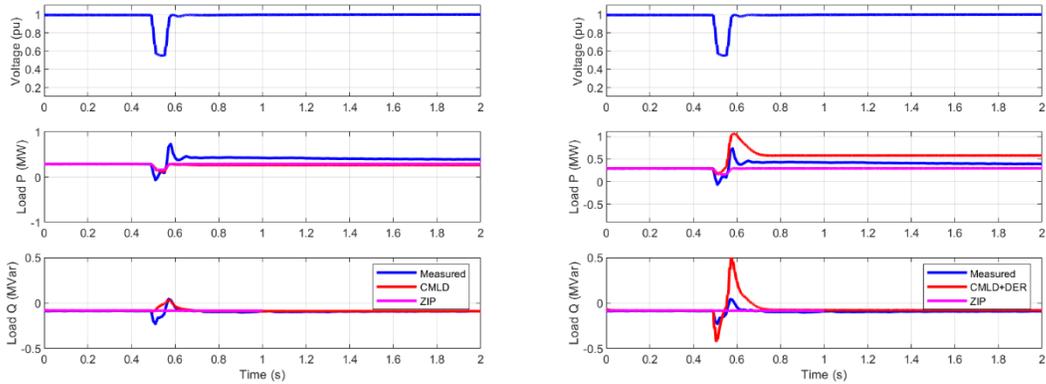
a) With CMLD only (residential composition)   b) With CMLD+DER (average composition)
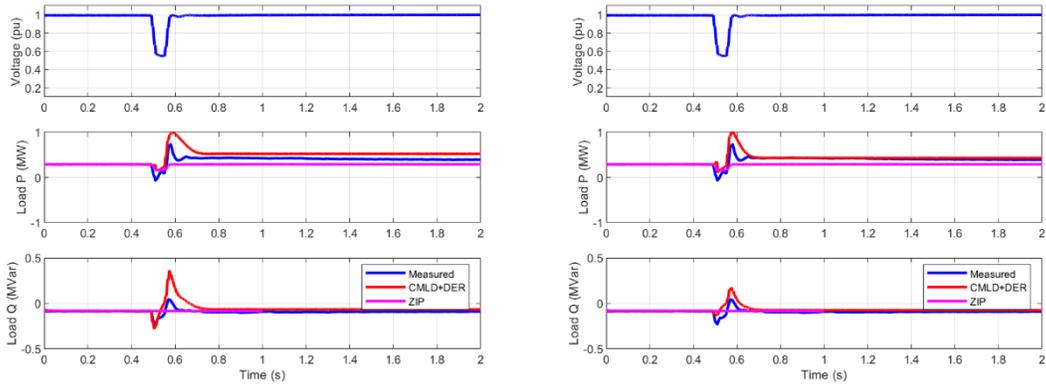
a) With CMLD+DER (residential composition)   b) With CMLD+DER (adjusted composition)

Figure 31: Comparison of a playback simulation for the Brendale 11A feeder event, with various model options.
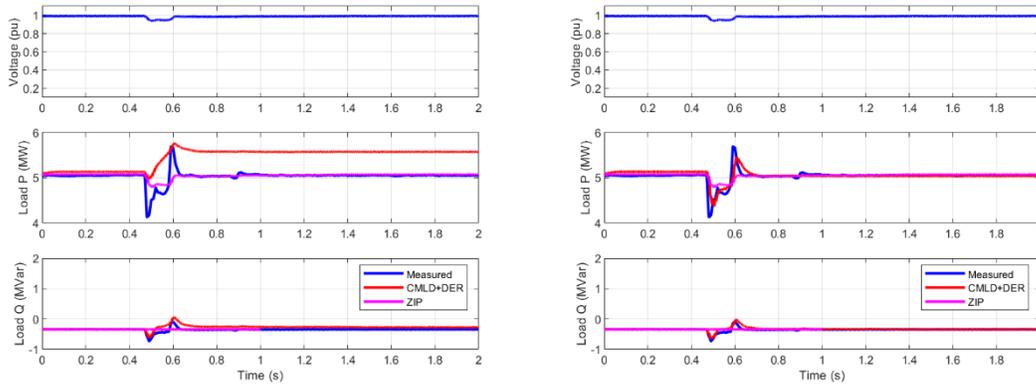
a) With CMLD+DER (residential composition)   b) With CMLD+DER (adjusted parameters)

Figure 32: Comparison of a playback simulation for the Currimundi feeder event, with various model options.

7.4   Observations and Conclusions from the Distribution Feeder Event Simulations

From the results of the distribution feeder events with DER on-line, it is event that:

1. The existing static-load model clearly does not capture the aggregated behavior of the load plus DER. This is of course no surprise.
2. The CMLD model alone is not able to emulate the measured behavior, as seen in Figure 31 a). Again, this is no surprise.
3. The combination of CMLD + DER_A, is able to reasonably emulate both the real and reactive power response, as measured, once we:
    a. start with the summer residential CMLD load composition, and then
    b. make some changes to the parameters.

To get the reasonable fits shown in Figure 31 d) and Figure 32 b), the adjustments made were different. In the case of Brendale 11A, the motor load composition was reduced, and the majority of the load was moved to power electronic load. For Currimundi the load composition was not changed, but rather the trip levels for the power electronic load and the trip time on the first trip setting for DER_A (*tl1*) were adjusted.

The conclusion that can thus be made is that the CMLD+DER_A model can indeed reasonably emulate the aggregated behavior of the load and DER on a distribution feeder. However, as seen with the two simple cases here, there can be considerable variation in the parameters in order to achieve a reasonable fit from case to case. This presents a challenge with coming up with system wide parameters, and again emphasizes the need for sensitivity analysis on the most influential parameters of the models, which are (i) the load composition parameters (fractions of various load components) and (ii) the trip settings on all the various load components and the DER. To be able to perform meaningful sensitivity analyses, more in-depth surveys of the present load and DER composition in the Australian system will be needed.

Finally, as a sanity check we ran one of the cases for the distribution feeder playback scenarios in GE PSLF™ as well, and confirmed the same result as Siemens PTI PSS®E

(see Figure 33). This gives further confidence that the beta model in Siemens PTI PSS®E is performing as expected.
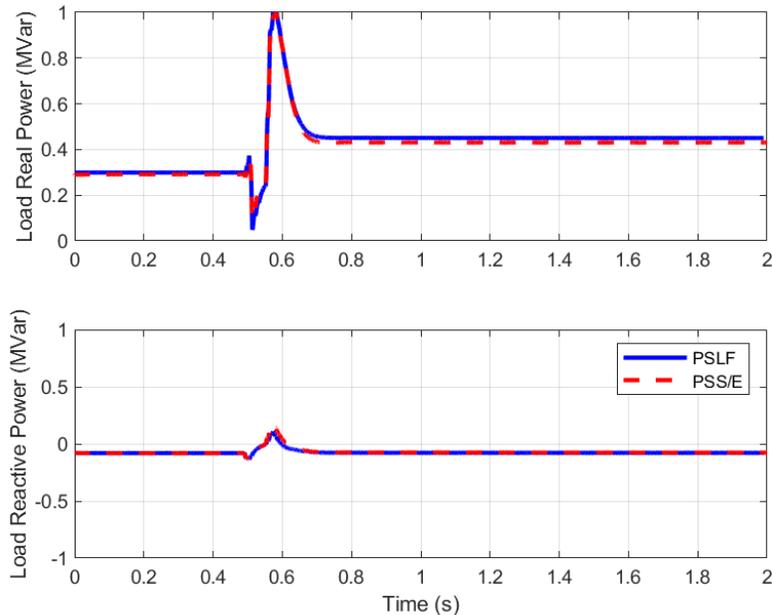
Figure 33: Comparison of a playback simulation for the Brendale 11A event as simulated in GE PSLF™ versus Siemens PTI PSS®E. The very small, almost visible, difference in the steady state value of power is likely due to some minor differences in the way the distribution feeder model (distribution transformer and feeder equivalent) are handled in the two programs due to the programing philosophies of the vendors, as identified in the recent benchmark testing of this model in North America (in June 2019).

7.5   Simulating a System Wide-Event

AEMO provided the snapshot Siemens PTI PSS®E power flow and dynamics data for one significant system wide event that occurred in Victoria on November 20, 2018. The event was the fault and tripping of the 220-kV line from Deer Park to Keilor. No further information was available for the event, thus we assumed that the fault occurred at the Deer Park end and that it was cleared at both ends in 3^{20} cycles.

To run the event using the existing AEMO static (ZIP) load model was quite straight forward. To setup the case to run with the CMLD load model and the CMLD**DGU2 (i.e. CMLD + DER_A) model took some time to setup. It is also pertinent to explain this process and the assumptions involved, to inform future efforts by AEMO to more reasonably and accurately model the DER.

AEMO   provided   a   spreadsheet   (*2019-04-15-Summary-all-sources.xlsx*)   which summarized the information presently available on the total "name-plate" installed capacity of PV at each of the modeled transmission and distribution buses in their Siemens PTI PSS®E model. In this spreadsheet, there are a number of nodes listed with very little

---

[20] Initially, the fault was simulated at 5 cycles clearing, however, after some iterative simulations it was apparent that a 3 cycle clearing more closely matches the measured data.

PV (less than 1 MW nameplate, in many cases less than 0.1 MW). We neglected all nodes with less and 1 MW PV installed – this amounts to a total of 13 MW out of a total of 6.8 GW across the system, so it is a reasonable simplifying assumption for the present moment.

Furthermore, for this event in Victoria, based on the best data presently available, AEMO estimated the following capacity factor for each region:

Table 5: PV capacity factors just prior to the November 20, 2018 Victorian event.

QLD North	QLD Central	QLD South	NSW	SA	VIC	TAS North	TAS South
52%	52%	51%	40%	43%	10%	14%	11%

Thus, we took these capacity factors for the time of the event and multiplied them by the total nameplate capacity at each individual bus (for the appropriate region) in the *2019-04-15-Summary-all-sources.xlsx*, and thus estimated that at the time of the event there should have been a total of 2.542 GW of PV on-line.

As a next step, the entire load table in the power flow case for the whole eastern Australian system was exported from the Siemens PTI PSS®E EMS snapshot case into a RAW file. Then using Excel and automatically cross comparing this RAW file and the PV capacity calculation spreadsheet[21], all of the buses where PV should be installed were found. Of the more than 280 buses listed in the original spreadsheet from AEMO (*2019-04-15-Summary-all-sources.xlsx*), just over 160 were found that were in-service loads in the Siemens PTI PSS®E power flow model. This amounted to about 1.3 GW of PV. This was discussed with AEMO and they indicated that significant more work will be needed in the near future to be able to better associated the installed capacity of PV with the appropriate bus numbers in the Siemens PTI PSS®E power flow cases. So, at this time, the agreed to approach to get the amount of PV on-line in this event case was to scale everything by a factor of 2, to bring the total to 2.6 GW.

This was done, and using the RDCH activity in Siemens PTI PSS®E, the data was read back into the power flow case. It is important to explain one example record, just to be clear on the sequence of actions.

Consider row 1 of the spreadsheet *2019-04-15-Summary-all-sources.xlsx*. In this row it is stated that there is 34.18 MW of nameplate installed PV capacity at Abermain in Queensland South, and this should all be modeled on bus number 41365 in the power flow case. For this event, the capacity factor for Queensland South is 51%. Therefore, we have $0.51 \times 34.18 = 17.43$ MW on-line. However, as mentioned above, since all the PV buses could not be found, in order to keep the total in the system for this event at the total estimated value of 2.6 GW, each of the PV models added had to be scaled by a factor of two. Therefore, we must at $2 \times 17.43 = 34.86$ MW of DG at bus 41365. This is done as shown below:

---

[21] Using the VLOOKUP function in Excel.

Table 6: DG data entry into the power flow case.

Zone Num	Zone Name	Owner Num	Owner Name	In Service	Scalable	Interruptible	Pload (MW)	Qload (Mvar)	IPload (MW)	IQload (Mvar)	YPload (MW)	YQload (Mvar)	Distributed Gen (MW)	Distributed Gen (Mvar)	Distributed Gen Mode	G
47		1		☑	☑ Yes	☐ Yes	2.9030	0.7750	0.0000	0.0000	0.0000	0.0000	1.4200	0.0000	On	☐
40		1		☑	☑ Yes	☐ Yes	1.4830	0.7750	0.0000	0.0000	0.0000	0.0000	0.0000	0.0000	Off	☐
47		1		☑	☑ Yes	☐ Yes	50.337	5.0860	0.0000	0.0000	0.0000	0.0000	34.8600	0.0000	On	☐
40		1		☑	☑ Yes	☐ Yes	15.477	5.0860	0.0000	0.0000	0.0000	0.0000	0.0000	0.0000		☐

Namely, we must:

1. Enter the 34.86 MW of DG into the column entitled "Distributed Gen (MW)"
2. Here it is assumed that all DG is operating at unity power factor; therefore the "Distributed Gen (Mvar)" column is left as 0.
3. The DG must be turned on (Distributed Gen Mode).
4. The load at the bus must be increased by this same amount. The original load (Pload) at this bus was 15.476 MW, and it has now been increased to 50.337 MW (15.476 + 34.86). This is to ensure that the original power flow solution remains the same. Namely, it is our assumption that 34.86 MW of PV was on-line, and thus the 15.476 MW in the original EMS snapshot was the net (not gross) load.

One final step was taken prior to running the simulations. The buses that include DG were placed in new zones, as follows:

1. Zone 48 – all QLD loads lumped up onto the EHV buses
2. Zone 47 – all QLD loads lumped onto distribution buses (11, 22 and 33 kV)
3. Zone 28 – all NSW loads lumped up onto the EHV buses
4. Zone 27 – all NSW loads lumped onto distribution buses (11, 22 and 33 kV)
5. Zone 38 – all VIC loads lumped up onto the EHV buses
6. Zone 37 – all VIC loads lumped onto distribution buses (11, 22 and 33 kV)
7. Zone 58 – all SA loads lumped up onto the EHV buses
8. Zone 57 – all SA loads lumped onto distribution buses (7.5, 11 and 33 kV)
9. Zone 78 – all TAS loads lumped up onto the EHV buses
10. Zone 76 – all TAS loads lumped onto distribution buses (11, 22, 33 and 44 kV)

With the above said, the CMLD**DGU2 records (per Appendix C and the load composition in section Table 1) were created for each of these Zones, together with the CMLD**U2 records used previously in section 6.1, and the event was simulated. The results are shown in Figure 34 and Figure 35.

The results are not highly conclusive, but it must be considered that due to a lack of presently available information there were a number of assumptions that had to be made, as outlined above. Nonetheless, the following conclusions can be made:

1. The existing static (ZIP) load model again depicts a snappy and quick return of the system voltage, with some sharp over-voltages. This is not seen in the measured system response.
2. The general slower recovery rate and more smooth response of the CMLD+DER_A model is more believable, and as the composition parameters are improved in the future, they may render even more promising results.
3. The exact timing, location and impedance of the fault has probably not been accurately modeled. However, there is little information available on these details.

4. The combined CMLD + DER_A model behaved well in the simulation and did not significantly affect the simulation time for simulating the event as compared to the existing static load model.

A final note is that the DER_A parameters used here where those representing PV installations post-2015 which are assumed to conform with the 2015 AEMO standards (see Appendix 4, column 7 of the table). As AEMO embarks on using the CMLD**DGU2 model, a more detailed survey of the deployment of DG on the AEMO system will be needed to both better quantify the amount and location of PV, as well as the exact mix of PV characteristics (i.e. those that conform to the performance requirements of the 2015 standard and those that do not). Thus, the appropriate initial parameters as suggested in Appendix B will need to be used, and refined as more experience is gained. Furthermore, note that the present AEMO NEM model is severely lacking in proper turbine-governor modeling for the vast majority of the synchronous generation fleet on the system. This deficiency of the Australian system model will need to be first addressed before one can rely on any results that may pertain to system wide frequency events. This is why frequency response events related to the DER_A model were not investigated here.
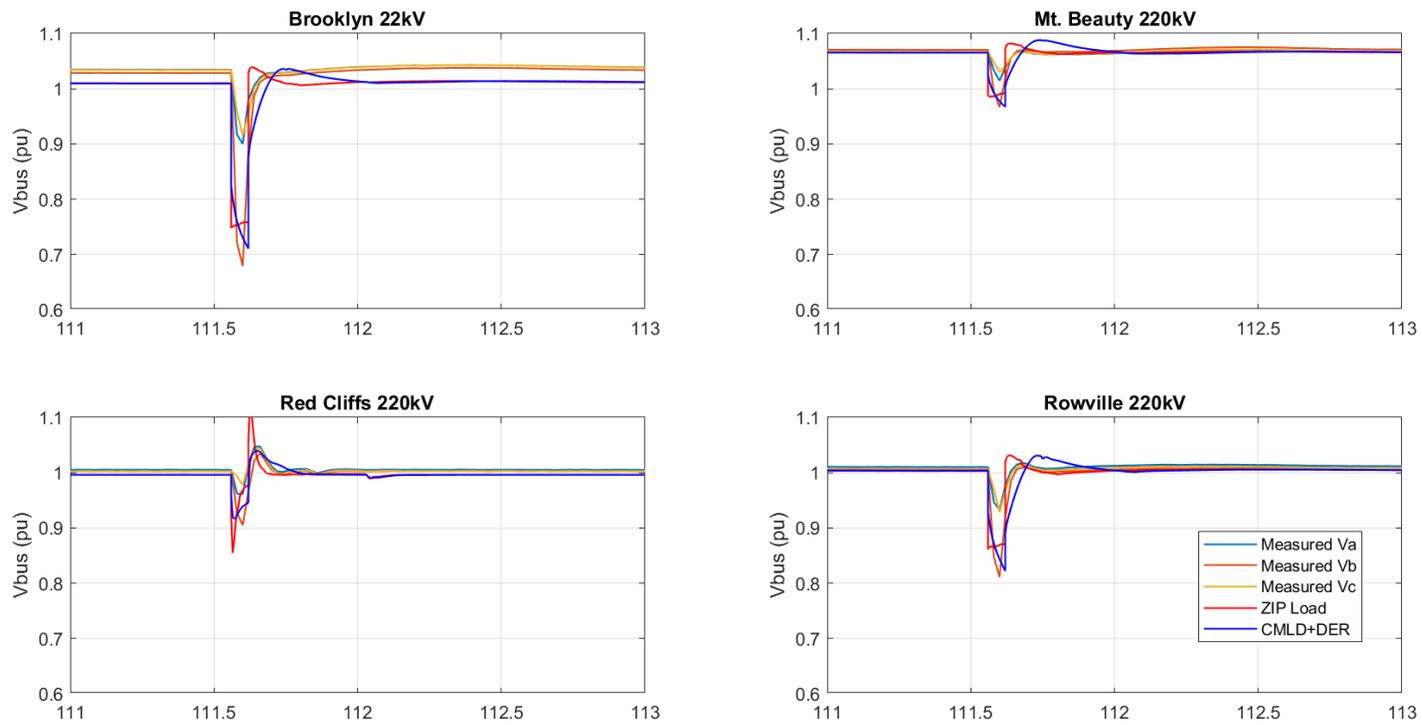
Figure 34: Comparison of a simulation to measurement at key EHV buses for the Victorian event. Simulated a fault (with significant fault impedance) and tripping of the Deer Park to Kielor 220 kV line.
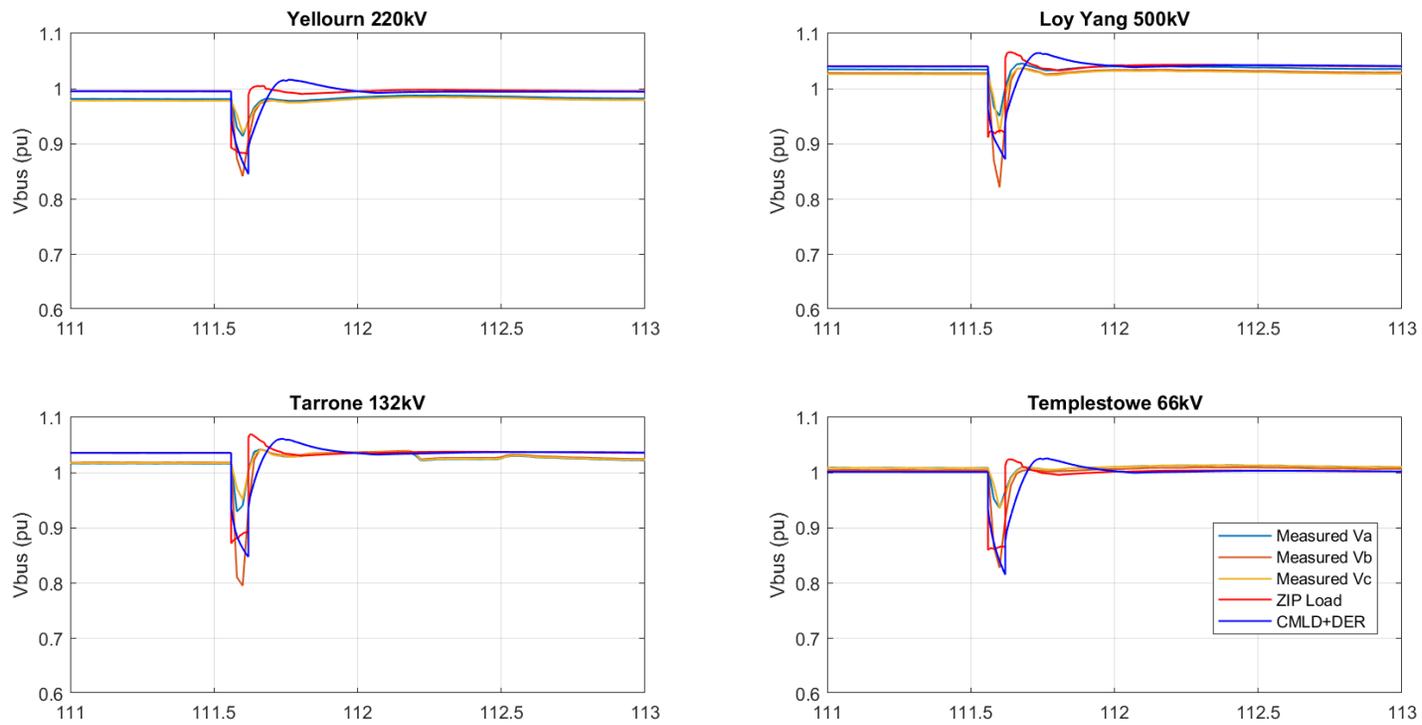
Figure 35: Comparison of a simulation to measurement at key EHV buses for the Victorian event. Simulated a fault (with significant fault impedance) and tripping of the Deer Park to Kielor 220 kV line.

8.   Conclusions and Future Work

The development of a composite load model with both dynamic and static load components has been achieved, based on the data provided by AEMO. Furthermore, the so-called DER_A (distributed energy resource model A) has also been used and incorporated into the composite load model. The model when applied across the entire Australian NEM runs well, shows no issues, and simulations for several system disturbances do not result in a significantly longer simulation time.

Moreover, simulations were performed comparing the performance of the composite load (CMLD) model to the existing AEMO static (ZIP) load model for simulating events recorded on three (3) distribution feeders, and for two (2) large system events.

The results from the distribution feeder simulations show that the CMLD model gives a much closer match of the actual load response, particularly in the reactive power (Q) response of the loads. These simulations also clearly show that the key factors in the CMLD model that have a significant influence on the performance of the model are (i) the composition numbers (i.e. what fraction of the load falls into each of the six major load components, motor A, B, C, D, power electronic and static load), and (ii) the trip settings for the various load components (i.e. the motor loads and the power electronic load).

The results from the large system disturbances also show that the CMLD model results more closely match actual system performance. However, as illustrated by some more onerous simulations (i.e. simulating bolted 3-phase faults at EHV buses) the CMLD model can result, in some cases, in seeing a fault-induced delayed voltage recovery where the EHV voltages can take up to 1 second to recover to their pre-fault levels. This delayed voltage recovery is due to the stalling of the Motor D component of the CMLD model. Moreover, based on research and development in North America, the stalling of these so-called Motor D type loads is driven by many factors, some of which cannot be truly captured in a positive-sequence simulation tool such as Siemens PTI PSS®E. For example, the rate at which the voltage drops, the point-on-wave where the fault occurs, the type of mechanical load and the configuration of transformer windings (i.e. Y-Delta etc.) can all influence what the actual motors see at their terminals down at the low voltage levels where these type motors are used, and thus drive if and how the motor stalls. As such, in the end some level of sensitivity analysis is needed when trying to capture the potential for delayed voltage recovery. Motor D type loads represent singe-phase capacitor-start induction motors that are used in residential and light-commercial loads such as air-conditioning, refrigeration, heat-pumps etc. Based on the initial survey and data mining done by AEMO, the percentage of such loads (Motor D component) has been estimated at between 3 to 6% across Australia. This is because, it is believed that the majority of air-conditioning load in Australia is inverter-based (i.e. similar to power electronic loads). Thus, again this highlights the need for more investigation in the future in understanding the actual load composition today and how it might evolve in the near future in Australia.

Thus, in summary it may be said that the CMLD load model does make simulations more closely match measured system response, but in addition when modeling 3-phase faults (as is done typically in transmission planning studies, while in real-life 3-phase fault are rare) the simulation results for system voltage recovery will be more pessimistic with the CMLD model than they have been in the past with the existing AEMO static-load model.

The CMLD model has been available in Siemens PTI PSS®E (and several other simulation platforms in North America) for several years. The standalone DER_A model has also been available in these commercial tools, and tested in North America, for close to a year. However, the combination of the two models into a single comprehensive aggregated model to represent both load and DER at the end of an aggregate feeder was just very recently (early June, 2019) tested as a beta version across the North American simulation tools within the WECC Modeling and Validation Working Group. As such, this combined model that was used here for simulating the combination of CMLD and DER_A, is based on the latest beta release from Siemens PTI PSS®E in Version 34.5.1.

Thus, the combination of CMDL and DER_A was then used to simulate a few distribution-feeder events and one large system wide event.

For the distribution events, it was seen that a relatively good match could be achieved with the combination of the CMDL + DER_A model, with some adjustment to the parameters. This includes seeing the DER momentarily blocking and then coming back up, and some possibly tripping, as seen in real events. Of course, the ZIP model (nor the CMLD model by itself) cannot emulate any of this behavior.

For the system wide event, the key observations were that: (i) the existing static (ZIP) load model again depicts a quick return of the system voltage, with some sharp over-voltages, that do not resemble the actual measured system behavior, (ii) that the general slower recovery rate and more smooth response of the CMLD+DER_A model is more believable, and as the composition parameters are improved in the future, they may render even more promising results, and (iii) the combined CMLD + DER_A model behaved well in the simulation and did not significantly affect the simulation time for simulating the event as compared to the existing static load model.

All of the above said, the following general conclusions and recommendations can be made:

- To improve the parameterization of the CMLD and DER_A models, AEMO should consider doing a more thorough and up-to-date (i.e. based on 2018 data perhaps) survey of the loads in the Australian system, and/or working with entities like the CSIRO to come-up with more up-to-date composition data on the residential and commercial loads across the regions in Australia, and if possible at a little more granular level – e.g. based on general climate zones.
- To thus update the load composition percentages, and come up with percentages for a wider range of seasons/times of the year and times of the day for planning studies.
- To try to explicitly model large industrial loads such as mining where this is plausible and more specific and detailed data on such loads can be obtained.
- To perform sensitivity analysis to identify the key parameters that the Australian system is most sensitive to in the CMLD model, and to thus in the process of the surveying identify physically meaningful boundaries and ranges on these parameters. Based on the limited analysis here, and some engineering judgment, it can be said at a first cut that the most sensitive parameters are, the composition

fractions (*Fma, Fmb, Fmc, Fmd, Fel*) and the trip settings on the various load components.

- To survey in more depth the installed PV throughout the system and to be able to clearly cross-reference the installed capacity with the specific power flow bus numbers in the base cases developed. Also, a process needs to be put in place to regularly monitor and update these as PV installations continue to increase. Furthermore, it would be beneficial to develop some simple automated routines to generate the PV records and populate them into the power flow records (see what needs to be done as described in section 7.4) to simplify this process. Moreover, the DER_A parameters used here where those representing PV installations post-2015 (for the sake of simplicity). As AEMO embarks on using the CMLD**DGU2 model, and performs more detailed surveys of the deployment of DG on the AEMO system, attention should also be given to identifying the exact mix of PV characteristics (i.e. those that meet the 2015 performance requirements and those that do not). Thus, the appropriate parameters will need to be used, and refined as more experience is gained.

- The present AEMO NEM Siemens PTI PSS®E model is severely lacking in proper turbine-governor modeling for the vast majority of synchronous generators on the system. This deficiency of the Australian system model will need to be first addressed before one can rely on any results that may pertain to system wide frequency events.

- Given the fact that AEMO performs many of its studies in EMT modeling tools (i.e. PSCAD), particularly for low system short-circuit strength regions, it may be prudent to develop an aggregated DER model, similar to DER_A, in the PSCAD environment, as well as the CMLD type aggregate load model structure. This would need some significant time to develop and test and benchmark.

- To take a closer look at the distribution parameters of the CMLD model for each region in the Australian NEM system.

- There may be value in introducing more high-speed monitoring (e.g. digital-fault recorders, which are PMU capable) both at load centers, as well as at key transmission nodes and generating station in order to increase the fidelity of the measured event data for future refinement of models through comparing simulations to measured event data.

Finally, it should be emphasized, as illustrated even by the initial work here, that there can never be "one" highly accurate load model, due to the constantly changing nature of the load and the countless variety of load components, as well as the variability in the PV generation. Thus, when performing planning studies, a level of sensitivity analysis needs to be performed around both load model composition and the load component trip settings. Such sensitivity analysis, must however, incorporate engineering judgement in that (i) variations in the composition numbers should be based on survey data to ensure that unrealistic numbers are not used, and (ii) sensitivity analysis may only be needed when looking at the most onerous system conditions and contingencies.

For futuristic planning studies AEMO may need to consider working with consultants and firms with expertise in solar forecasting, in order to develop realistic PV penetration scenarios under various potential weather patterns for system planning studies.

References

[1] *NERC Technical Reference Document: Dynamic Load Modeling,* December 2016. https://www.nerc.com/comm/PC/LoadModelingTaskForceDL/Dynamic%20Load%20Modeling%20Tech%20Ref%202016-11-14%20-%20FINAL.PDF

[2] A. M. Gaikwad, R. J. Bravo, D. Kosterev, S. Yang, A. Maitra, P. Pourbeik, B. Agrawal, R. Yinger, and D. Brooks, "Results of Residential Air Conditioner Testing in WECC", *Proceedings of the IEEE PES General Meeting, Pittsburg*, July 2008. https://ieeexplore.ieee.org/document/4596549

[3] "Proposal for DER_A Model," June 19, 2019. https://www.wecc.org/Reliability/DER_A_Final_061919.pdf

[4] US Department of Energy Report, "Commercial Building Motor Protection Response Report", by D. James and J. Kueck, June 2015; Report Number PNNL--24468

[5] *End-Use Data Development for Power System Load Model in New England - Methodology and Results*, Lawrence Berkeley National Laboratory, Subcontract No. 7071126, Date: April 10, 2014 https://certs.lbl.gov/sites/all/files/data-development-for-ne-end-use-load-modeling.pdf

[6] A. Maitra, A. Gaikwad, P. Pourbeik and D. Brooks, "Load Model Parameter Derivation Using an Automated Algorithm and Measured Data", *Proceedings of the IEEE PES General Meeting*, Pittsburg, July 2008. https://ieeexplore.ieee.org/abstract/document/4596333

[7] D. Ramasubramanian, P. Mitra and A. Gaikwad, "VFD Model Development", Presentation at the WECC MVWG, November 2018. https://www.wecc.org/_layouts/15/WopiFrame.aspx?sourcedoc=/Administrative/VFD%20Modeling-%20Ramasubramanian.pdf&action=default&DefaultItemOpen=1

Appendix A – Default Parameters of the CMLDXXU2 Model

In the 3-phase motor parameters below the values of *T'o* and *T''o* are the same as those used in the typical/default values used in North America. It should be noted that since the Australian system is a 50 Hz, versus the North American system which is a 60 Hz system, technically speaking one would have to scale these motor time constants by a factor of 1.2 (60/50). However, this has not been done here since these are "generic" parameters, and the influence of such a small change is perhaps negligible. The torque speed curve calculations in Figure 3, actually uses the values below on a 50 Hz base.

In the table below, of the CMLD model parameters, the color codes have the following general meanings:

1. The most sensitive parameters (i.e. those that likely vary the most, and will have the some of the most significant impact of system performance) are the ORANGE colored parameters. These are the load composition parameters. These need to be derived from a good understanding of the actual load composition (as described in section 4) and a reasonable range identified.
2. The GREEN parameters pertain to the trip settings of the Motor A, B, C and the power electronic loads. These also will have a marked effect on voltage recovery as they impact the amount of load that will trip (and/or recover) during and post fault for particularly severe (3-phase) faults. For *Vd1* a typical range is between 0.85 to 0.7 (but may be as high as 0.9 for extremely sensitive electronic loads) and *Vd2* may range from 0.6 to 0.5. Again, some load surveying, particularly for industrial loads may be needed to get a better handle of the typical range of voltage trip settings for the large 3-phase motors in Australia. One should remember that all these parameters represent aggregated response and so eventually some engineering judgment is needed in playing sensitivities with these numbers.
3. The light BLUE parameters pertain to the typical distribution system configuration (e.g. if distribution transformers have an active OLTC or not, and what the typical aggregated feeder impedances are on the systems). Again, it should be noted that this is an aggregate model, and furthermore in real-life all of the load is not at the end of the feeders, but rather distributed along the feeder. So once again engineering judgement is needed in tweaking the equivalent aggregate distribution feeder impedance. The key point is to have a reasonable number, with a reasonable expected X/R ratio at the distribution level.
4. The GREY parameters represent the aggregated electrical characteristics of the load components, and in general these are not changed since many of them were developed from laboratory tests of individual component testing (e.g. the Motor D parameters are based off of extensive laboratory testing of residential a/c loads in the US [2] for a/c systems that use single-phase capacitor-start induction motors).

CON	Parameter Name	Default Value	Comments/Description
J	Load MVA Base	-0.8	Load Factor = |Load MW / MVA Base|
J+1	Substation shunt B	0	These are assumed typical parameters for the singel equivalent distribution feeder
J+2	Rfdr	0.04	and the distribution transformer, on the MVA base of the load, in per unit. Rfdr/Xfdr
J+3	Xfdr	0.04	is the feeder resistance/reactance. The amount of explicit shunt capacitors at the
J+4	Fb	0.75	substation is set to 0. Fb is the fraction of the feeder shunt compensation (internally
J+5	Xxf	0.08	calcualted by the model that is place at the substation side of the feeder. Xxf is the
J+6	Tfixhs	1	transformer leakage reactance, and Tfixhs and Tfixls are the fixed tap positions on the
J+7	Tfixls	1	high/low side windings of the transformer.
J+8	LTC	1	The on-load tap-changer (OLTC) is assumed to be active.
J+9	Tmin	0.9	These are the assumed typical range of the the OLTC taps. Numbers were indicated to
J+10	Tmax	1.1	be reasonable by AEMO for the Australian system. The values are the minimum tap
J+11	Step	0.0063	(Tmin), maximum tap (Tmax) and individual tap steps (Step).
J+12	Vmin	1	These are the assumed typical range of voltage control and timings for the OLTC.
J+13	Vmax	1.02	Numbers were indicated to be reasonable by AEMO for the Australian system. TD is
J+14	TD	30	the initial delay before taps start to move, and TC is the delay between subsequent
J+15	TC	5	tap adjustments. Vmin/Vmax is the range in which the distribution bus voltage is to
J+16	Rcmp	0	Current compensation on the OLTC control; typically set to zero.
J+17	Xcmp	0	
J+18	FmA		Fraction of load that is Motor A
J+19	FmB		Fraction of load that is Motor B
J+20	FmC		Fraction of load that is Motor C
J+21	FmD		Fraction of load that is Motor D
J+22	Fel		Fraction of load that is Power Electronic Load
J+23	Pfel	1	Power Electronic load power factor; assumed to be unit at the end-use load level
J+24	Vd1	0.7	Vd1 is the voltage below which electronic load starts to drop until it all drops out at
J+25	Vd2	0.5	Vd2. These values are in per unit and the drop off is linear between these two values.
J+26	PFs	1	
J+27	P1e	1	The static-load model. It is given by the following equation:
J+28	P1c		$P = P_o * (P1c * (V/V_o) P1e + P2c * (V/V_o) P2e + P3) * (1 + Pfrq * \Delta f)$
J+29	P2e	2	$Q = Q_o * (Q1c * (V/V_o) Q1e + Q2c * (V/V_o) Q2e + Q3) * (1 + Qfrq * \Delta f)$
J+30	P2c		$P_o = P_{load} (1. - F_{ma} - F_{mb} - F_{mc} - F_{md} - Fel)$
J+31	Pfrq	0	$Q_o = P_o * \tan(\operatorname{acos}(PFs))$
J+32	Q1e	1	$P3 = 1. - P1c - P2c$
J+33	Q1c		$Q3 = 1. - Q1c - Q2c$
J+34	Q2e	2	
J+35	Q2c		
J+36	Qfrq	-1	

CON	Parameter Name	Default Value	Comments/Description
J+37	MtypA	3	Motor A Electrical Parameters (all other 3-phase motors)
J+38	LFmA	0.75	
J+39	RaA	0.04	
J+40	LsA	1.8	
J+41	LpA	0.12	
J+42	LppA	0.104	
J+43	TpoA	0.095	
J+44	TppoA	0.0021	
J+45	HA	0.1	
J+46	etrqA	0	
J+47	Vtr1A	0.65	Assume motor trip settings (remember this is an aggregated model)
J+48	Ttr1A	0.1	
J+49	Ftr1A	0.2	
J+50	Vrc1A	0.1	
J+51	Trc1A	9999	
J+52	Vtr2A	0.5	
J+53	Ttr2A	0.02	
J+54	Ftr2A	0.75	
J+55	Vrc2A	0.65	
J+56	Trc2A	0.1	
J+57	MtypB	3	Motor B Electrical Parameters (3-phase fans motors)
J+58	LFmB	0.75	
J+59	RaB	0.03	
J+60	LsB	1.8	
J+61	LpB	0.19	
J+62	LppB	0.14	
J+63	TpoB	0.2	
J+64	TppoB	0.0026	
J+65	HB	0.5	
J+66	etrqB	2	
J+67	Vtr1B	0.55	Assume motor trip settings (remember this is an aggregated model)
J+68	Ttr1B	0.02	
J+69	Ftr1B	0	
J+70	Vrc1B	0.65	
J+71	Trc1B	0.05	
J+72	Vtr2B	0.5	
J+73	Ttr2B	0.025	
J+74	Ftr2B	0	
J+75	Vrc2B	0.6	
J+76	Trc2B	0.05	
J+77	MtypC	3	Motor C Electrical Parameters (3-phase pump motors)
J+78	LFmC	0.75	
J+79	RaC	0.03	
J+80	LsC	1.8	
J+81	LpC	0.19	
J+82	LppC	0.14	
J+83	TpoC	0.2	
J+84	TppoC	0.0026	
J+85	HC	0.1	
J+86	etrqC	2	
J+87	Vtr1C	0.58	Assume motor trip settings (remember this is an aggregated model)
J+88	Ttr1C	0.03	
J+89	Ftr1C	0	
J+90	Vrc1C	0.68	
J+91	Trc1C	0.05	
J+92	Vtr2C	0.53	
J+93	Ttr2C	0.03	
J+94	Ftr2C	0	
J+95	Vrc2C	0.62	
J+96	Trc2C	0.1	

CON	Parameter Name	Default Value	Comments/Description
J+97	Tstall	0.03	Time it takes for the 1-phase induction motor to stall
J+98	Trestart	0.3	Time it takes for the 1-phase induction motor to restart
J+99	Tv	0.025	Filter time constant
J+100	Tf	0.1	Filter time constant
J+101	CompLF	1	Loading factor = MW/MVA Base = 1.0
J+102	CompPF	0.98	Assume slightly inductive load
J+103	Vstall	0.45	Voltage below which 1-phase motor stalls
J+104	Rstall	0.1	
J+105	Xstall	0.1	
J+106	Lfadj	0	
J+107	Kp1	0	
J+108	Np1	1	
J+109	Kq1	6	Motor D Stall Representation - average values dervied from laboratory testing in North America (reference [2])
J+110	Nq1	2	
J+111	Kp2	12	
J+112	Np2	3.2	
J+113	Kq2	11	
J+114	Nq2	2.5	
J+115	Vbrk	0.86	
J+116	Frst	0.2	Assumed restart capability for 1-phase motors
J+117	Vrst	0.95	
J+118	CmpKpf	1	Frequency dependency
J+119	CmpKqf	-3.3	
J+120	Vc1off	0.5	Contactor tripping and reclosing - matches/similar to other motor protection values
J+121	Vc2off	0.4	
J+122	Vc1on	0.6	
J+123	Vc2on	0.52	
J+124	Tth	15	
J+125	Th1t	0.7	
J+126	Th2t	1.9	
J+127	Fuvr	0.1	...ection settins for 1-phase a/c motor (e.g. thermal time constant of bi-metalic contactor
J+128	UVtr1	0.5	
J+129	Ttr1	0.02	
J+130	UVtr2	0.1	
J+131	Ttr2	9999	
J+132	Ferst	0.8	Assumed restart capability for electronic loads

Appendix B – Default Parameters for the DER_A Model

Parameter	Units	Description	Parameters to implement in the NEM				Notes
			Inverters installed pre-2015	Inverters installed post-2015	Inverters with Volt-Var enabled	Parameter Values Used in This Study	
Trv	s	transducer time constant (s) for voltage measurement	0.02	0.02	0.02	0.02	A reasonable minimum value is 20ms (1/50Hz) - measure once every cycle.
Trf	s	transducer time constant (s) for frequency measurment (must be ≥ 0.02 s)	0.02	0.02	0.02	0.02	A reasonable minimum value is 20ms (1/50Hz) - measure once every cycle.
dbd1	pu	lower voltage deadband ≤ 0 (pu)	-1	-1	-0.083333	-1	For voltag/var enabled based on NEM standard
dbd2	pu	upper voltage deadband ≥ 0 (pu)	1	1	0.041667	1	For voltag/var enabled based on NEM standard
Kqv	pu/pu	proportional voltage control gain (pu/pu)	0	0	5.169231	0	For voltag/var enabled based on NEM standard
Vref0	pu	voltage reference set-point > 0 (pu)	1	1	1	1	Defines where the deadband is across. By default is 1.
Tp	s	transducer time constant (s)	0	0	0	0	Neglect in order to disable PI control and effect simple proportional droop.
Tiq	s	Q control time constant (s)	0.02	0.02	0.02	0.02	Reasonable minimum value. Emulates delays in controls.
Ddn	%	frequency control droop gain ≥ 0 (down-side)	0	28.6	28.6	28.6	Based on NEM standard; for reducing power during over-frequency.
Dup	%	frequency control droop gain ≥ 0 (up-side)	0	0	0	0	Not enabled (for increasing power for under-frequency)
fdbd1	pu	lower frequency control deadband ≤ 0 (pu)	-1	-0.005	-0.005	-0.005	Per NEM standard, only respond for over-frequneyc if frequency goes above 50.25 Hz.
fdbd2	pu	upper frequency control deadband ≥ 0 (pu)	1	1	1	1	Do not respond for under-frequency.
femax	pu	frequency control maximum error ≥ 0 (pu)	99	99	99	99	Neglect. More useful for PI control (typically in large plants).
femin	pu	frequency control minimum error ≤ 0 (pu)	-99	-99	-99	-99	Neglect. More useful for PI control (typically in large plants).
Pmax	pu	Maximum power (pu)	1	1	1	1	Set to default (1 pu = rated power). **Note:** if under-frequency response is ever enabled it is very important to set this value to the maximum available incident solar energy at the time being simulated.
Pmin	pu	Minimum power (pu)	0	0	0	0	Default setting.
dPmax	pu/s	Power ramp rate up > 0 (pu/s)	99	0	0	0	Per NEM standard there is a hysteresis effect when PV responds to over-freqeuncy, such that for at least 60 seconds the power is not allowed to increase once freqeuncy goes below 50.15 Hz. To "emulate" this, make dPmax = 0 in order to prevent model from increasing power back up, once decreased by droop action.
dPmin	pu/s	Power ramp rate down < 0 (pu/s)	-99	-99	-99	-99	Set at a large negative value to allow to drop P very fast.
Tpord	s	Power order time constant (s)	0	0	0	0	Neglect - no PI control
Kpg	%	active power control proportional gain	0	0	0	0	Neglect - no PI control
Kig	%	active power control integral gain	10	10	10	10	Will effect proportional droop with 0.1 s time lag (100ms time constant).
Imax	pu	Maximum converter current (pu)	1	1	1	1	This is the maximum current rating of the inverter = 1 in pu.
vl0	pu	voltage break-point for low voltage cut-out of inverters	0.85417	0.75	0.75	0.75	Based on NEM standard.
vl1	pu	voltage break-point for low voltage cut-out of inverters	0.9725	0.9725	0.9725	0.9725	Based on NEM standard.
vh0	pu	voltage break-point for high voltage cut-out of inverters	1.10417	1.104167	1.104167	1.104167	Based on NEM standard.
vh1	pu	voltage break-point for high voltage cut-out of inverters	1.08333	1.083333	1.083333	1.0833	Based on NEM standard.
tvl0	s	timer for vl0 point	2	2	2	2	Based on NEM standard.
tvl1	s	timer for vl1 point	0.1	0.1	0.1	0.1	Based on NEM standard.
tvh0	s	timer for vh0 point	2	0.2	0.2	0.2	Based on NEM standard.
tvh1	s	timer for vh1 point	1.5	1.5	1.5	1.5	Based on NEM standard.
vrfrac	%	fraction of device that recovers after voltage comes back to within vl1 < V < vh1	0.2	0.2	0.2	0.2	Initial guess, that only 20% recovers.
fl	Hz	frequency break-point for low frequency cut-out of inverters	47.5	47	47	47	Per NEM standard.
fh	Hz	frequency break-point for high frequency cut-out of inverters	52.5	52	52	52	Per NEM standard.
tfl	s	timer for fl (Tfl > Trf)	1	1.5	1.5	1.5	If frequency goes below fl for more than tfl seconds, then the entire model will trip.
tfh	s	timer for fh	1	0.2	0.2	0.2	If frequency goes above fh for more than tfh seconds, then the entire model will trip. Do not use a small number to avoid erroneous tripping on frequency. Check results if a fault is placed nearby due to problems in calculating frequency at or near a faulted bus in positive-sequence programs.
Tg	s	Current control time constant	0.02	0.02	0.02	0.02	Typical minimum value for large scale staility studies. Could set to zero. Better to have a time constant.
rrpwr	pu/s	Power rise ramp rate following a fault > 0 (pu/s)	10	10	10	10	As quickly as possible (10pu/s - almost immediately). Nothing defined in standard.
Tv	s	time constant on the output of the voltage/frequency cut-out	0.02	0.02	0.02	0.02	Typical value.
Vpr	pu	voltage below which frequency tripping is disabled	0.7	0.7	0.7	0.7	Reasonable value, to attempt to get rid of frequency calculation problem.
Pflag	flag	0 - for constant Q control, and 1 - constant power factor control	1	1	1	1	If power factor control is selected (Pflag = 1), then pfaref is calculated internally by the software program as arctan(Qgeno/Pgeno), where Qgeno and Pgeno are the initial real and reactive power output of the model, respectively, as determined by the initial power flow solution.
Pqflag	flag	0 - Q priority, 1 - P priority for current limit	0	0	0	0	Q priority
Freq_flag	flag	0 - frequency control disabled, and 1 - frequency control enabled	0	1	1	1	Enable freqeuncy control (to allow over-freqeuncy response)
Ftripflag	flag	0 - frequency tripping disabled; 1 - frequency tripping enabled	1	1	1	1	Enable.
Vtripflag	flag	0 - voltage tripping disabled; 1 - voltage tripping enabled	1	1	1	1	Enable.
typeflag	flag	0 - the unit is a generator Ipmin = 0; 1 - the unit is a storage device and Ipmin = - Ipmax	0	0	0	0	All PV (no storage)
Xe	pu	Source impedance reactive > 0 (pu)	0.3	0.3	0.3	0.3	The decision at the last REMTF meeting was to introduce a basic voltage source representation at the model interface to the network to avoid potential numerical problems. This requires only one additional parameter Xe. Since this is an aggregated model, the resistance of the source impedance is neglected, and Xe should be set to a value typically between 0.2 to 0.4 pu. May have to tweak if numerical problems observed.
Iqh1	pu	Maximum limit of reactive current injection, p.u.	0	0	0.3	0	Current injection limits for voltage/var control.
Iql1	pu	Maximum limit of reactive current injection, p.u.	0	0	-0.3	0	Current injection limits for voltage/var control.

Appendix C – Parameters for the CMLD**DGU2 Model

Important Note: the parameter list below is the parameter list for the CMLD**DGU2 model in its current beta version format as available in Siemens PTI PSS®E Version 34.5.1, upon request from Siemens PTI. This model has been extensively tested and benchmark in the WECC MVWG in North America. However, once the final model is released in a future official release of Siemens PTI PSS®E, Siemens PTI has indicated that the parameter list will be refined such that the order of parameters for the CMLD part of the model is harmonized (in the same or similar order) as the existing CMLD**U2 model. As such, some reordering of the parameter list below may be needed once this model is employed in the official release of the model.

CONS	Value	Description
J+0	-0.8	LBASE, Load MVA Base
J+1	0	Bsub, Substation compensation B, pu on load MVA base
J+2	0.04	Rfdr, Feeder resistance, pu on load MVA base
J+3	0.04	Xfdr, Feeder reactance, pu on load MVA base
J+4	0.08	Xxfr, Transformer reactance, pu
J+5	1	Tfixhs, Fixed taps on high side
J+6	1	Tfixls, Fixed taps on low side
J+7	1	LTC, Flag (1 – active; 0 – disabled)
J+8	0.9	Tmin, Minimum tap
J+9	1.1	Tmax, Maximum tap
J+10	0.00625	Tstep, tap step
J+11	1	Vmin, User setting of min voltage
J+12	1.02	Vmax, User setting of max voltage
J+13	30	TD, Delay before first tap move
J+14	5	TC, Delay between tap moves
J+15	0	Rcomp, Compensating resistance for tap adjustment
J+16	0	Xcomp, Compensating reactance for tap adjustment
J+17		FmA, Fraction of motor A
J+18		FmB, Fraction of motor B
J+19		FmC, Fraction of motor C
J+20		FmD, Fraction of motor D
J+21		Fel, Fraction of electronic load
J+22	1	PFel, Power factor of electronic load
J+23	0.7	Vd1, V where electronic load starts to decrease
J+24	0.5	Vd2, Voltage at which electronic load is gone
J+25	0.8	Ferst, Fraction of elect load that can restart
J+26	1	PFs, Power factor of static load
J+27	1	P1e, First exponent for static load
J+28		P1c, First fraction for static load
J+29	2	P2e, 2nd exponent for static load
J+30		P2c, 2nd fraction for static load
J+31	0	Pfrq, Frequency coefficient for static load
J+32	1	Q1e, First exponent for reactive static load

CONS	Value	Description
J+33		Q1c, First fraction for reactive static load
J+34	2	Q2e, 2nd exponent
J+35		Q2c, 2nd fraction
J+36	-1	Qfrq, frequency coefficient for reactive part
J+37	0.75	LFmA, Motor A Ratio of power to base
J+38	0.04	Ra, Motor A Armature resistance
J+39	0.0832	Xa, Motor A leakage reactance
J+40	1.8	X, Motor A Synchronous reactance
J+41	0.12	X", Motor A Transient reactance
J+42	0.104	X", Motor A Subtransient reactance
J+43	0.095	To", Motor A Transient open circuit time constant
J+44	0.0021	To", Motor A Subtransient open circuit time constant
J+45	0.1	H, Motor A Inertia constant
J+46	0	etrq, Motor A Load torque exponent for speed
J+47	0.65	Vtr1, Motor A 1st undervoltage trip voltage, pu
J+48	0.1	Ttr1, Motor A 1st undervoltage trip delay, s
J+49	0.2	Ftr1, Motor A 1st undervoltage trip fraction
J+50	0.1	Vrc1, Motor A 1st undervoltage reclose voltage, pu
J+51	9999	Trc1, Motor A 1st undervoltage reclose delay, s
J+52	0.5	Vtr2, Motor A 2nd undervoltage trip voltage, pu
J+53	0.02	Ttr2, Motor A 2nd undervoltage trip delay, s
J+54	0.75	Ftr2, Motor A 2nd undervoltage trip fraction
J+55	0.65	Vrc1, Motor A 2nd undervoltage reclose voltage, pu
J+56	0.1	Trc2, Motor A 2nd undervoltage reclose delay, s
J+57	0.75	LFmB, Motor B Ratio of power to base
J+58	0.03	Ra, Motor B Armature resistance
J+59	0.112	Xa, Motor B leakage reactance
J+60	1.8	X, Motor B Synchronous reactance
J+61	0.19	X", Motor B Transient reactance
J+62	0.14	X", Motor B Subtransient reactance
J+63	0.2	To", Motor B Transient open circuit time constant
J+64	0.0026	To", Motor B Subtransient open circuit time constant
J+65	0.5	H, Motor B Inertia constant
J+66	2	etrq, Motor B Load torque exponent for speed
J+67	0.55	Vtr1, Motor B 1st undervoltage trip voltage, pu
J+68	0.02	Ttr1, Motor B 1st undervoltage trip delay, s
J+69	0	Ftr1, Motor B 1st undervoltage trip fraction
J+70	0.65	Vrc1, Motor B 1st undervoltage reclose voltage, pu
J+71	0.05	Trc1, Motor B 1st undervoltage reclose delay, s
J+72	0.5	Vtr2, Motor B 2nd undervoltage trip voltage, pu
J+73	0.025	Ttr2, Motor B 2nd undervoltage trip delay, s
J+74	0	Ftr2, Motor B 2nd undervoltage trip fraction
J+75	0.6	Vrc1, Motor B 2nd undervoltage reclose voltage, pu
J+76	0.05	Trc2, Motor B 2nd undervoltage reclose delay, s

CONS	Value	Description
J+77	0.75	LFmC, Motor C Ratio of power to base
J+78	0.03	Ra, Motor C Armature resistance
J+79	0.112	Xa, Motor C leakage reactance
J+80	1.8	X, Motor C Synchronous reactance
J+81	0.19	X", Motor C Transient reactance
J+82	0.14	X", Motor C Subtransient reactance
J+83	0.2	To", Motor C Transient open circuit time constant
J+84	0.0026	To", Motor C Subtransient open circuit time constant
J+85	0.1	H, Motor C Inertia constant
J+86	2	etrq, Motor C Load torque exponent for speed
J+87	0.58	Vtr1, Motor C 1st undervoltage trip voltage, pu
J+88	0.03	Ttr1, Motor C 1st undervoltage trip delay, s
J+89	0	Ftr1, Motor C 1st undervoltage trip fraction
J+90	0.68	Vrc1, Motor C 1st undervoltage reclose voltage, pu
J+91	0.05	Trc1, Motor C 1st undervoltage reclose delay, s
J+92	0.53	Vtr2, Motor C 2nd undervoltage trip voltage, pu
J+93	0.03	Ttr2, Motor C 2nd undervoltage trip delay, s
J+94	0	Ftr2, Motor C 2nd undervoltage trip fraction
J+95	0.62	Vrc1, Motor C 2nd undervoltage reclose voltage, pu
J+96	0.1	Trc2, Motor C 2nd undervoltage reclose delay, s
J+97	1.0	CompLF, Motor D real power to motor base ratio
J+98	0.86	Vbrk, Motor D "break-down" voltage
J+99	0.98	CompPF, Motor D power factor at 1.0 pu voltage
J+100	0.45	Vstall, Motor D stall Voltage, pu
J+101	0.03	Tstall, Motor D stall delay time, s
J+102	0.95	Vrst, Motor D restart voltage after stall, pu
J+103	0.3	Trstrt, Motor D restart from stall delay time, s
J+104	0.2	Frst, Motor D frct that can restart after stall
J+105	0.1	Rstall, Motor D stall R, pu of motor base
J+106	0.1	Xstall, Motor D stall X, pu of motor base
J+107	1	CmpKpf, Motor D real power frequency dependency
J+108	-3.3	CmpKqf, Motor D reactive power freq dependency
J+109	0	LFadj, Adjustment to stall & breakdown voltage
J+110	0	Kp1, Motor D P coeff when voltage > Vbrk
J+111	1	Np1, Motor D P exp when voltage > Vbrk
J+112	6	Kq1, Motor D Q coeff when voltage > Vbrk
J+113	2	Nq1, Motor D Q exp when voltage>Vbrk
J+114	12	Kp2, Motor D P coeff when voltage < Vbrk
J+115	3.2	Np2, Motor D P exp when voltage < Vbrk
J+116	11	Kq2, Motor D Q coeff when voltage < Vbrk
J+117	2.5	Nq2, Motor D Q exp when voltage<Vbrk
J+118	0.025	Tv, Motor D V time constant for contactors, s
J+119	0.1	Tf, Motor D f time constant for contactors, s
J+120	0.5	Vc1off, Motor D V contactors start opening, pu

CONS	Value	Description
J+121	0.4	Vc2off, Voltage all contactors have dropped out
J+122	0.52	Vc2on, Voltage contractors start to reclose
J+123	0.6	Vc1on, Voltage at which all contactors reclose
J+124	15	Tth, Motor D heating time constant
J+125	0.7	Tth1, Motor D temperature tripping begins, pu
J+126	1.9	Tth2, Motor D temperature completely tripped
J+127	0.1	Fuvr, Motor D fraction with undervoltage relays
J+128	0.5	Vtr1, Motor D 1st undervoltage pick-up, pu
J+129	0.02	Ttr1, Motor D 1st undervoltage trip delay, s
J+130	0.1	Vtr2, Motor D 2nd undervoltage pick-up, pu
J+131	9999	Ttr2, Motor D 2nd under voltage trip delay, s
J+132	0.02	Trv, DER V measurement transducer time constant
J+133	0.02	Trf, DER frequency measurement transducer time constant
J+134	-1	Vdb1, DER lower voltage deadband (< 0)
J+135	1	Vdb2, DER upper voltage deadband
J+136	0	Kqv, DER voltage error gain after deadband
J+137	1	Vrefo, DER initial ref V, used if close to Vt
J+138	0	Tp, DER power measurement time constant
J+139	0.02	Tiq, DER State(K+2) Iq time constant
J+140	28.6	Ddown, DER reciprocal of droop for over-frequency
J+141	0	Dup, DER reciprocal of droop for under-frequency
J+142	-0.005	fdb1, DER lower frequency control deadband
J+143	0	fdb2, DER upper frequency control deadband
J+144	99	femax, DER max value of power error
J+145	-99	femin, DER min value of power error
J+146	1	Pmax, DER Maximum power limit
J+147	0	Pmin, DER Minimum power limit
J+148	0	dPmax, DER Power reference maximum ramp rate
J+149	-99	dPmin, DER Power reference minimum ramp rate
J+150	0	Tp, DER Power filter time constant
J+151	0	Kpg, DER PI controller gain
J+152	10	Kig, DER PI controller integral gain
J+153	1	Imax, DER Maximum converter current
J+154	0.75	vl0, DER V lower break-point on P vs V curve
J+155	0.9725	vl1, DER V upper break-point on P vs V curve
J+156	1.10417	vh0, DER V higher break-point on P vs V curve
J+157	1.0833	vh1, DER V lower break-point on P vs V curve
J+158	2	Tl0, DER timer value for vlo
J+159	0.1	Tl1, DER timer value for vl1
J+160	0.2	Th0, DER timer value for vho
J+161	1.5	Th1, DER timer value for vh1
J+162	0.2	Vfrac, DER power fraction on recovery
J+163	47	fl, DER lower frequency for tripping (Hz)
J+164	52	fh, DER upper frequency for tripping (Hz)

CONS	Value	Description
J+165	1.5	Tfl, DER timer value for low frequency tripping
J+166	0.2	Thf, DER timer value for high frequency tripping
J+167	0.02	Tg, DER time constant for id and iq filter
J+168	10	Rrwpr, DER id ramp rate limit
J+169	0.02	Tv, DER time constant on power multiplier output
J+170	0.7	Vflow, DER low voltage frequency trip limit
J+171	0	Iqh1, DER max limit on reactive current injection
J+172	0	Iql1, DER min limit on reactive current injection
J+173	1	pf, DER power factor
J+174	1	LF, DER ratio of load to rating
J+175	0	Fder, DER fraction of load (for Version 33; ignore)
J+176	0.3	Xe, DER output reactance

ICONS	Value	Description
M+0	0	Used internally for data checking
M+1	0	Used internally for data checking
M+2	1	pfFlag, power factor control if 1, else Q control
M+3	1	FreqFlag, Frequency effect on P if = 1
M+4	0	PQFlag, P priority (1), Q priority (0)
M+5	1	GenFlag, Generator (1) or storage device (0)
M+6	1	VtripFlag, Enable voltage tripping (1)
M+7	1	FtripFlag, Enable frequency tripping (1)
M+8	1	Q mode, For Version 33